Phytomedicine Plus 4 (2024) 100550

Contents lists available at ScienceDirect

Phytomedicine Plus

journal homepage: www.sciencedirect.com/journal/phytomedicine-plus

Liquid chromatography–mass spectrometry and xCELLigence real time cell analyzer revealed anticancer and antioxidant metabolites in *Trianthema portulacastrum* L. (Aizoaceae)

Muhali Olaide Jimoh [a,b,*], Mahboob Adekilekun Jimoh [c], Nasifu Kerebba [d], Olalekan Olanrewaju Bakare [e], Comfort Titilayomi Senjobi [a], Sefiu Adekilekun Saheed [f], Rose Kadye [g], Earl Prinsloo [g], Charles Petrus Laubscher [a]

[a] *Department of Plant Science, Olabisi Onabanjo University, Ago-Iwoye, 120107, Nigeria*
[b] *Department of Horticultural Sciences, Cape Peninsula University of Technology, Bellville, 7535, South Africa*
[c] *Department of Plant Biology, Osun State University, P.M.B. 4494, Osogbo, 210001, Nigeria*
[d] *Department of Chemistry, Makerere University, Kampala, 7062, Uganda*
[e] *Department of Biochemistry, Olabisi Onabanjo University, Sagamu, 121102, Nigeria*
[f] *Department of Botany, Obafemi Awolowo University, Ile-Ife, 220005, Nigeria*
[g] *Biotechnology Innovation Centre, Rhodes University, Makhanda, 6140, South Africa*

ARTICLE INFO

Keywords:
Aizoaceae
Anticancer metabolites
Black pigweed
Cancer-related deaths
Chronic diseases
Phenolic compounds

ABSTRACT

Background: The rising incidence of cancer is a major concern globally being a leading cause of early mortality in most countries. This burden is projected to increase to 28.4 million cases worldwide by 2040 and yet, may be worsened by continuous exposure to risk factors due to a sheer shift from consumption of natural nutrients. To reverse this trend, it is imperative to source novel anticancer metabolites from plants that could minimize carcinogenic effects by suppressing the proliferation and survival of cancer cells.
Purpose: This study aimed at characterizing and quantifying index anticancer and antioxidant metabolites, in the cultivars of *T. portulacastrum.*
Methods: The Ultra-High Performance Liquid Chromatography Mass Spectroscopy (UHP-LCMS) was used to quantify and characterize index anticancer and antioxidant metabolites in shoot, root and whole plant extracts of *Trianthema portulacastrum* (T01,T02,T03,T04,T05,T06). The biological activity of the tested samples was monitored on the xCELLigence Real Time Cell Analyzer to determine the cytotoxicity of the extracts as a function of cell index at a specific time post dose using the concentration range of 0.16–2.5 %.
Results: Based on the responses observed 48 h post exposure, all extracts showed high levels of cytotoxicity as determined by the xCELLigence apart from the root extracts. Rapid decreases in cell index (CI) values observed at higher extract percentages are highly indicative of cell death. These biological activities may be attributed to different anticancer metabolites such as epigallocatechin, glucaric acids, byakangelicin, xanthotoxin, apaensin, acetoxy-6-gingerol among other compounds of significant therapeutic benefits that were quantified with UHP-LCMS.
Conclusion: These findings suggest that *T. portulacastrum* contains diverse anticancer metabolites which could be leveraged to develop plant-based anticancer drugs or novel chemicals with extended therapeutic utility.

Abbreviations: AME, accurate mass error; CI, cell index; CID, collision induced dissociation; CO_2, carbon iv oxide; DMSO, Dimethylsulfoxide; ECEGCG, (epi) catechin-(epi)gallocatechin gallate; ECIS, Electric Cell-Substrate Impedance Sensing; ESI, Electrospray ionization; IC_{50}, 50 % inhibitory concentration; ICH, International Conference on Harmonization; LC–MS, Liquid Chromatography–Mass Spectrometry; LOD, limit of detection; LOQ, limit of quantification; MMP-9, matrix metalloproteinase-9; MS, mass spectrometry; NIST, National Institute of Standards and Technology; PAs, proanthocyanidins; RDA, retro Diels Alder; RSD, relative standard deviation; RTCA-SP, Real Time Cell Analyzer Single Plate system; T01, *T. portulacastrum* shoot (white flower); T02, *T. portulacastrum* shoot (purple flower); T03, *T. portulacastrum* whole plant (white flower); T04, *T. portulacastrum* whole plant (purple flower); T05, *T. portulacastrum* root (white flowered); T06, *T. portulacastrum* root (purple flower); TPP, Techno Plastic Products; UHPLC-MS, Ultra-High Performance Liquid Chromatography Mass Spectroscopy; UV–VIS, Ultraviolet-visible.

* Corresponding author.
E-mail addresses: muhali.jimoh@oouagoiwoye.edu.ng, jimohm@cput.ac.za (M.O. Jimoh).

https://doi.org/10.1016/j.phyplu.2024.100550

Available online 24 March 2024

1. Introduction

The hallmark of cancer lies in the alteration of extracellular matrix that maintains the functional and structural integrity of tissues and organs in the body (Cox, 2021; Reiser, 2007). As a result of this alteration, the biomechanical and biochemical architecture of the matrix becomes defective resulting in malignant tumor (Cox, 2021). In 2020, new cases of cancer estimated at 19.3 million were recorded globally with attendant 10.0 million cancer-related deaths. This burden is projected to increase to 28.4 million cases worldwide by 2040 and yet, may be worsened further by continuous exposure to risk factors orchestrated by industrialization, globalization and a shift from natural nutrients consumption (Sung et al., 2021). Therefore, the rising incidence of cancer is a major concern globally being a leading cause of early mortality in most countries irrespective of their Human Development Index (Bray et al., 2021; Seraphin et al., 2021). This has called for concerted efforts from all and sundry to propagate effectively, cancer management and prevention measures especially in developing countries with limited access to adequate healthcare (Bray et al., 2021; Fadelu and Rebbeck, 2021).

Earlier, chemotherapeutic and radiotherapeutic methods were employed in the management of cancer (Davis et al., 2019). These approaches target cancer cells and kill them directly. However, patients are left with grave consequences after treatment (Kruger et al., 2019). For instance, gonadal failure has been attributed to the administration of chemotherapeutic agents and radiotherapeutic effects although the testis was reported to be more vulnerable than the ovary (Howell and Shalet, 1998; Wei and Crowne, 2019; Zavattaro et al., 2021). Other radiotherapy and chemotherapy-induced dysfunctions include cardiotoxicity, hematopoietic system injury, hepatotoxicity, gastrointestinal toxicity, oral mucositis, neurotoxicity and nephrotoxicity (Zhang et al., 2018). Recent advances in biology and technology have transformed cancer treatment. These advances include identification and generation of oncogenic drivers, and oncogenic deaddiction, leading to oncogene targeted therapies (Altmann, 2018; Arnedos et al., 2014). Nevertheless, the success of oncogene targeted therapies is limited by the barricade of immune checkpoints, genomic instability and intratumor heterogeneity which are the root cause of developing resistance to cancer treatment (Arnedos et al., 2014; Pardoll, 2012). Application of high throughput technologies and biomarkers for cancer treatment has made possible a thorough assessment of the genetic profile of cancer cells, thereby guiding medical initiatives aimed at cancer diagnosis and treatment decisions (Arnedos et al., 2014; Davis et al., 2019).

It has been widely reported in literature that plants produce novel anticancer metabolites such as bioactive O-Prenyl secondary metabolites, acetylenic metabolites, coumarin derivatives (Detsi et al., 2017; Genovese et al., 2015; Kontogiorgis et al., 2012; Siddiq and Dembitsky, 2008) and other marine-based anticancer drugs (Jimeno et al., 2004; Nigam et al., 2019). These metabolites which are majorly products of secondary metabolism offer extended therapeutic utility, but could minimize carcinogenic effects by suppressing the proliferation and survival of cancer cells as well as transforming the growth factors or modulating signal transduction pathways which define the invasiveness of malignant cells (Choudhari et al., 2020; Detsi et al., 2017).

The use of Liquid Chromatography–Mass Spectrometry (LC–MS) technique in profiling secondary metabolites in plants has been widely reported (Idris et al., 2023). Given its enhanced characterization efficiency, the Ultra High Performance LC–MS is built to separate complex mixture of diverse chemicals in botanical materials (Wu et al., 2013). The xCELLigence Real Time Cell Analyzer Single Plate system is an electronic detector which monitors the biological activity of a tested natural product at a particular time (Hamidi et al., 2017). The system may be employed in extrapolating the chemical profiles of anticancer metabolites in a plant sample from a standard compound of known activity (Stefanowicz-Hajduk and Ochocka, 2020). This will make possible, the determination of cytotoxicity of plant extracts as a function of cell index at a specific time post dose calculated using the sigmoidal dose.

Trianthema portulacastrum, Olowonjeja, Akisan (Yoruba, Southwestern Nigeria), or black pigweed, giant pigweed, desert horse purslane is a diffusely branched annual plant with glabrous leaves (Falade et al., 2019; Royal Botanic Gardens, 2023). It belongs to Aizoaceae, the common ice plant family that is endemic to South Africa but commonly found in India, sub-Sahara Africa, tropical America, Southern China, Southeast and West Asia (Gaddeyya and Kumar, 2015; Sunder et al., 2010). In African continent, the plant is widely distributed in Togo, Ivory Coast, Egypt, Gambia, Senegal, and Nigeria where it is often regarded as an invasive weed, and largely underutilized (Dogara et al., 2020; Shaltout et al., 2013). *Trianthema portulacastrum* is an important herb in Indian diets and commonly utilized for preparing Ayurvedic drugs (Mandal and Bishayee, 2015; Sukalingam et al., 2017). Different parts of *T. portulacastrum* are used for the treatment of breast cancer, food poisoning, corneal ulcers, cardiac diseases, piles, and traditionally used as analgesic, laxatives, alexiteric, and anti-inflammation (Hussain et al., 2011; Igoli et al., 2005; Mandal and Bishayee, 2015). A recent study revealed that *T. portulacastrum* exhibited in vitro cytotoxicity to HIV (Jimoh et al., 2024).

Some chemical constituents of *T. portulacastrum* identified with some analytical methods include betacyanin, p-methoxybenzoic acid, 5-hydroxy-2-methoxybenzaldehyde, leptorumol, 5,2′-dihydroxy-7-methoxy-6,8-dimethylflavone, 3,4-dimethoxy cinnamic acid, 3-acetylaleuritolic acid and trianthenol (Shivhare et al., 2012; Sukalingam et al., 2017). Additionally, analytical LC–MS analysis method was performed on *T. portulacastrum* samples previously to identify a handful of compounds such as β-sitosterol, trianthenol, ferulic acid, 2^1,5-dihydroxy-7-methoxy-6,8-dimethylflavone, 20-hydroxyecdysone, β-sitosterol glycoside, leptorumol (Abuzaid et al., 2020) and indeed with complete analysis. The study further carried out in vitro studies of the isolated compounds against human hepatocellular carcinoma cell lines (Abuzaid et al., 2020). Despite this useful information and the diverse phytoconstituents and immense pharmacological usage of *T. portulacastrum*, previous knowledge is only limited to the analysis of one or a few classes of marker constituents, and the reported analytical methods are inadequate for the comprehensive quality control of *T. portulacastrum*, its phytochemistry and its preparations for antioxidant and anticancer activities for potential use as a natural source of anticancer compounds. This study aimed at presenting UHP-LC–MS analytical method that comprehensively characterizes many index anticancer and antioxidant metabolites, quantification of the metabolites thereof, profiling of the cultivars of *T. portulacastrum* and assessing plant samples using the xCELLigence Real Time Cell Analyzer to monitor the anticancer effects to complement existing therapies for cancer prevention and management. There could also be concerns where their exist chemical variation with in the cultivars of *T. portulacastrum* and there for implications on the biological activities. In this study we have also characterized the chemical constituents of the cultivars and perhaps implications on the anticancer and antioxidant activities.

2. Materials and methods

2.1. Plant collection and preparation

Fresh parts of the two biotypes of *T. portulacastrum* (Fig. 1) were harvested from the backyard of Olorubu Central Mosque, Olaiya Community, off Awo Road, Ede, Osun State, Southwestern Nigeria (7° 45' 11" N, 4° 25' 34" E). The plant specimen was deposited at the IFE herbarium in Department of Botany, Obafemi Awolowo University, Ile-Ife, Nigeria and allocated a voucher number IFE-18,184 accordingly. After collection, the plant samples were separated into three distinct parts; leaves, whole plant, and roots for the two biotypes, resulting in six (6) different samples which were labelled T01, T02, T03, T04, T05 and T06 accordingly (Table 1). The plant samples were oven-dried to a constant weight at 35 °C and pulverized with an electric blender. The pulverized

Fig. 1. (A) *T. portulacastrum* shoot (white flower), (B) *T. portulacastrum* shoot (purple flower).

plant samples were kept in airtight bottles which were refrigerated for further use.

2.2. Extraction procedure

Twenty grams of the pulverized plant was weighed in a round bottom flask containing 500 mL ethanol. The mixture was shaken vigorously at 120 rpm on an orbital shaker (Orbital Incubator Shaker, Gallenkamp) for two days, and run through a Whatman No. 1 filter paper fixed in a Buchner funnel. This suction force for the filtration process was generated by a vacuum pump connected to the Buchner funnel. Excess ethanol in the filtrate was sucked out with a rotary evaporator (Strike-202 Steroglass, Italy) kept at 78 °C until the crude extract became concentrated and dry (Jimoh et al., 2019).

2.3. Cell culture and maintenance

The cervical cancer cell model HeLa was used to determine the cytotoxicity of the extracts. Briefly, cultures were maintained in 75 cm^3 flasks (TPP, Switzerland) in basal medium consisting of Dulbecco's Modified Eagle's Medium (High Glucose), 10 % Foetal Calf Serum and antimycotic-antibiotic solution (all available from Gibco). Cultures were evaluated for *Mycoplasma* contamination using standard Hoechst 33,342 staining and fluorescence microscopy (Atale et al., 2014). Subculturing was performed using standard trypsinization and trypan blue enumeration (Filetti et al., 2020). Cells were incubated at 37 °C in a humidified 5 % CO_2 atmosphere.

2.4. The xCELLigence protocol

Extract cytotoxicity was evaluated using Electric Cell-Substrate Impedance Sensing (ECIS) on a xCELLigence Real Time Cell Analyzer Single Plate system (RTCA-SP) following solubilization in 100 % (v/v) dimethylsulfoxide (Sigma–Aldrich, St Louis) and centrifugation at 10 000 rpm to precipitate insoluble mass (Hamidi et al., 2017). Serial dilutions (5–0.08 %) were prepared in basal medium prior to extract addition following 24-hour cell settling and proliferation. Briefly, 50 µL of warmed basal medium was added to all wells for pre-equilibration and cells were enumerated and added at 20 000 cells per well in 100 µL volume. Extracts were prepared at 4:1 ratio to ensure appropriate dilution upon addition in 50 µl. Effects of extracts were monitored for a further 24–48 h of incubation. Cell index values were collected in 15 min increments. All ECIS runs were performed in E-Plate 96 plates (Agilent) in triplicate wells per extract dilution. Cytotoxicity was determined as Cell Index at a specific time post dose and calculated using the Sigmoidal Dose Response (Variable Slope). Cell Index vs Time plots were prepared using Graphpad Prism (v9).

Table 1
Plant sample codes and description for LC–MS characterization and xCELLigence assays.

S/N	Sample code	Sample description
1	T01	*T. portulacastrum* shoot (white flower)
2	T02	*T. portulacastrum* shoot (purple flower)
3	T03	*T. portulacastrum* whole plant (white flower)
4	T04	*T. portulacastrum* whole plant (purple flower)
5	T05	*T. portulacastrum* root (white flower)
6	T06	*T. portulacastrum* root (purple flower)

2.5. Identification of phytochemicals

2.5.1. Method for HPLC-DAD analysis

The profiling of the *T. portulacastrum* extracts was initially carried out using a HPLC-DAD (Agilent 1200 series USA) following a method previously reported and validated (Zeb, 2015). During profiling, the analysis was performed using a RP-18 HS C18 discovery column (150 mm x 4.6 mm i.d.; 5 µm, column temperature: room temperature). The mobile phase consisted of water containing 0.1 % Trifluoroacetic acid (A), MeOH containing 0.1 % Trifluoroacetic acid (B) and the flow rate was set at 1 mL/min. The gradient elution program composed of; 0 min 100 % A move to 100 % B after 25 min. The detection wavelength performed at three different UV channels; 280, 320 and 360 nm were chosen to monitor the run. The injection volume was 20 µL. The chromatograms are shown in the supporting information (S1).

2.6. Liquid chromatography–mass spectrometry (LC–MS) analysis of phytochemicals

Phytochemical analysis of *T. portulacastrum* extracts was done using a Waters Synapt G2 Quadrupole time-of-flight (QTOF) mass spectrometer (MS) connected to a Waters Acquity ultra-performance liquid chromatograph (UPLC) (Waters, Milford, MA, USA) was used for high-resolution UPLC-MS analysis. Electrospray ionization was used in negative and positive modes with a cone voltage of 15 V, a desolvation temperature of 275 °C, at 650 L/h, and the rest of the mass spectrometry (MS) settings optimized for the best resolution and sensitivity. The adducts of +H, +Na, +NH4 and -H, +Cl,+COOH were selected in positive ion mode and negative ion mode, respectively. Data was acquired by scanning from *m/z* 150–1500 in resolution mode as well as in MS^E mode. The retention time (RT) range was set at 0.1–15.0 min with tolerance of ±0.2 min. Two channels of MS data were captured in the MS^E mode, the first at a low collision energy (4 V), and the second at a collision energy ramp (40–100 V), which also allowed for the acquisition of fragmentation data. Leucine enkephalin was used as reference mass for accurate mass determination, and the instrument was calibrated with sodium formate. Separation was achieved on a Waters BEH C18, 2.1 × 100 mm, 1.7 µm column. An injection volume of 2 µL was used and the mobile phase consisted of water with 0.1 % formic acid (solvent A) and acetonitrile containing 0.1 % formic acid (solvent B). The gradient started at 100 % solvent A for 0.5 min and changed to 100 % B over 12 min in a linear way. It maintained at 100 %B for another 0.5 min. It then went to 100 % A over 0.5 min, followed by re-equilibration to initial conditions (100 %A) for 2 min with a total run time of 15 min. The flow rate was 0.4 mL/min, and the column temperature was maintained at 55 °C.

MassLynx™ software version4.1 (Waters,Milford,MA,USA) was used in the acquisition and processing of data. Data were converted from project files (.PRO) to NetCDF files (.CDF) using Databridge in MassLynx (Waters,Milford,MA)and imported into MZmine for data processing.The following values were changed for processing the Q-ToF data: *m/z* tolerance was set at 0.01or 10 ppm, and retention time tolerance was defined as 0.1 min. The peak areas for individual ions were exported from the data matrix and then processed. The combination of retention time (RT), the mass-to-charge ratio (*m/z*), and MS/MS data was utilized to predict unknown compounds.

Compounds were identified, and tentative names were assigned based on the criteria listed below. (i) Accurate mass match: the masses were matched in Metlin; Metlin; http://metlin.scripps.edu/index.php, MassBank (http://www.MassBank.jp/http://MassBank.normandata.

eu/) as described by Horai et al., (2010). All compounds whose accurate mass error (AME) was > 5 ppm were considered unidentified (Zubarev and Makarov, 2013). Mass fragmentation patterns (if available): In the aforementioned databases and others such NIST (http://chemdata.nist.gov/) (NIST, 2021), and ReSpect (http://spectra.psc.riken.jp/) (Sawada et al., 2012), the mass fragmentation patterns of the compounds are matched. Several phenolic compound standards such as catechin, caffeic acid, rutin, ferulic acid, phloridzin, among others were used to spike the samples under similar LC–MS conditions, and fragmentation patterns were compared to identify compounds based on the ionization modes, retention times, and mass fragmentation. Lastly, the number of carbon atoms in the peak: if isotope abundances were available, the carbon atoms were calculated. The predicted number of carbon atoms in the putatively identified compound was used to increase the accuracy of the annotations.

2.7. Validation of analytical protocols for UHPLC-MS method and quantification of samples using UPLC-QTOF-MS and HPLC-DAD

The developed UHPLC-MS method was validated with linearity curve, the limit of detection (LOD), the limit of quantification (LOQ), precision, and recovery according to ICH (International Conference on Harmonization) recommendations (Branch, 2005). Different concentrations of the standard mixture (3.9, 7.8, 15.6, 31.3, 62.5, 125.0, and 250.0 mg/L), were injected for quantification. The linearity of the calibration curve was checked by plotting the peak areas against the series of standard solution concentrations (mg/L) and determining the correlation coefficient using a linear regression model. Samples were injected at concentrations of 3.9, 7.8, 15.6, 31.3, 62.5, 125.0, and 250.0 mg/L. The linearity of the calibration curve was plotted and checked with the correlation coefficient, r, of the linear regression model when $r > 0.99$. The LODs and LOQs were estimated as 3.3 and 10 times the standard deviation of the blank/slope ratio of the calibration curve, respectively. The repeatability of *T. portulacastrum* samples was assessed by using intraday and interday variations and the relative standard deviation (RSD) was taken as a measure of precision. The intraday and interday variations were analyzed using six replicates during a single day and by duplicating the experiments on three consecutive days. The intraday repeatability of the retention times was achieved in the range of 0.13–3.19 %, whereas the interday repeatability was from 1.09 to 3.00 %. The intraday repeatability, which was expressed as % relative standard deviations of the total peak area, was between 0.33 and 0.90 %, whereas the interday repeatability was 1.01–1.14 %.

The recovery test was done by adding the known amounts of standards at low (>50 % of the known amounts), medium (same as the known amounts) and high (150 % of the known amounts) levels into samples to evaluate the accuracy of the method. This was applied in triplicate. For quantification, phenolic subclasses were distinguished using UV/VIS absorptions. The preliminary quantification was achieved with HPLC-DAD. UV detection wavelengths were chosen based on UV spectrum of the markers. The phenolic acids had strongest UV absorption at 300, 309 and 322 nm, whereas flavanones at 284, 330 nm, flavonols had 254, 255 and 354 nm, dihydrocalcones 284 nm and finally flavan-3-ol, at 278 nm. Compounds whose peak areas were above LODs and LOQs were considered for quantification.

3. Results

3.1. Determination of cytotoxicity of fractions T01-T06 with xCELLigence real time analyzer

Extract cytotoxicity was evaluated through real-time Electric Cell-Substrate Impedance Sensing (ECIS) using the HeLa cervical cancer model to determine relative half-maximal inhibitory constants (IC_{50}) for the fractions. Cells were allowed to settle and grow for 24 h prior to exposure to extracts T01-T06. Overlapping growth curves seen in the initial 24 h of the assay offer a clear indication that cell seeding was equal in each well (Fig. 3). Cell growth proceeded as expected prior to exposure to the extracts. As can be seen in Fig. 3, all extracts showed characteristic relative concentration dependencies, as their increasing relative concentrations increase the relative toxicity of the extract. The effect of the extracts were monitored following the initial 24 h for cellular proliferation. Large spikes (Fig. 3, T03-05) observed at 24 h are artifacts of the removal and replacement of the E-plate into the xCELLigence cradle and does not affect the toxicity monitoring. Rapid decreases in cell index (CI) values observed at higher extract percentages are highly indicative of cell death as the rapid reduction in electrical impedance measurement is an indication of a decrease in direct contact of the cellular monolayer with the surface; increases in CI represents the inverse of this. Based on the responses observed 48 h post exposure, the relative IC_{50} values were determined using the area under the curve analysis during this period using the concentration range of 0.16–2.5 %. Table 2 shows the calculated IC_{50} values determined for each extract with relative goodness of fit represented by the R^2 value. Apart from T05 and T06, all extracts showed high levels of cytotoxicity as determined by the xCELLigence. The potential effect of DMSO on the cytotoxicity cannot be negated although observation of CI vs time for 2.5 % (v/v) DMSO showed little toxicity (Fig. 2).

3.2. UHPLC-ESI-MS

In this study, UHPLC-ESI-MS enabled the detection of a total of 134 peaks (Table 2). The base peak chromatograms of *T. portulacastrum* extracts shown in Fig. 4 in the MS detection, which enabled phytochemical screening.

3.3. Qualitative analysis of compounds from T. portulacastrum

3.3.1. Identification of phenolic acids and their derivatives (Fig. 5)

3.3.1.1. Hydroxybenzoic acids. Six benzoic acid derivatives were identified at peaks 16, 17, 40, 53, 82, and 96 (Table 3). Peak 17 in positive ion mode showed isomeric protonated molecular ion, $[M+H]^+$ at *m/z* 153 and upon collision inductive dissociation (CID), fragments *m/z* 137 $[M+H–H_2O]^+$ was formed enabling tentative identification of compound belonging to protocatechuic acid (Spínola et al., 2014) . The compound in peak 16 is thus identified as dihydroxy benzoic acid derivative with major ions at *m/z* 151 that relates to dihydroxy benzoic acid while peak 40 as acetyl 4-hydroxybenzaldehyde (after loss of 44 Da for the carbondioxide to generate *m/z* 121) using NIST data base and literature. Peak 53 displayed $[M-H]^-$; *m/z* 187 corresponding to that of gallic acid monohydrate since its MS^2 fragmentation gave high intense peak ions at 169 $[M-H-H_2O]^-$; and *m/z* 125 $[M-H–H_2O–CO_2]$. Its derivative at peak 82 was identified as ethylgallate glucoside. Compound 96 was identified as acetoxy-6-gingerol with MS^2 fragments 319 due to losses of H_2O from the parent ion. The ions 277 ($[M-H_2O + H]^+$), and 305 ($[M-H_2O + H]^+$), in agreement with earlier report (Park and Jung, 2016). The MS^1 ions was *m/z* 295 and 323 respectively producing common fragment ion *m/z* 115 $[C_7H_{13}O]^+$ in MS^2 formed as a result of inductive cleavage of the side chain.

3.3.2. Hydroxycinnamic acids

In this study, 9 hydroxycinnamic acids have been identified (peaks 18, 21, 24, 27, 29, 32, 36, and 101) (Table 3). The peak 21 was identified as p-coumaric acid deoxyhexose after addition of 146 Da of deoxyhexose to *m/z* 163 ([coumaric acid-H]$^-$). Peak 24 showed fragment ions and uv absorption similar to that of p-coumaric acid deoxyhexose and thus it was identified as p-coumaric acid deoxyhexose derivative. Peak 32 was identified as A number of hydroxycinnamic acids were detected as phenylpropane glyceride class at peaks 18, 29, 36 and 101. They had fragmentation ions *m/z* 179 $[M-H-74]^-$ and *m/z* 161 $[M-H-92]^-$ were

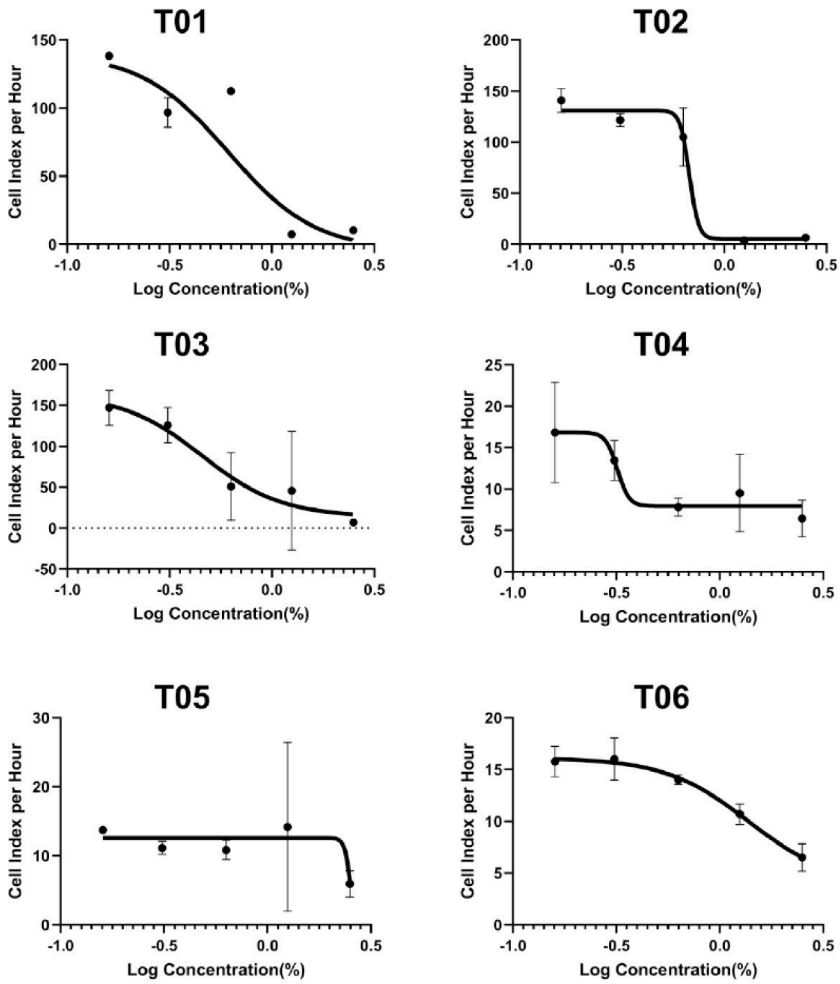

Fig. 2. Cell index per hour vs log concentration post dose.

characteristic loss of glycerol residue (Ma et al., 2007). The ions *m/z* 179, 161, 135, indicate the presence of a caffeoyl, *m/z* 193, 165 show a feruloyl while *m/z* 119, 109 is associated with coumaryl esterification. Thus peaks 18, 29 and 101 were identified as 1,3-O-dicoumaroylglycerol, 1,3-O-coumaroyl-feruloylglycerol and 1,3-O-feruloyl-caffeoylglycerol respectively. The ion at peak 36 showed fragments similar to that of 1,3-O-coumaroyl-feruloylglycerol so it was tentatively identified as 1,3-O-coumaroyl-feruloylglycerol derivative. One isomeric phenylpropenoic acid glucoside (PPAG) detected at peak 27 showed characteristic ion fragments at *m/z* 179, 119, 89, 161 (Table 3).

3.3.3. *Identification of flavonoids*

O-type flavonoid glycosides identification showed homolytic cleavage of its O-glycosidic bond leading to neutral loss of the sugar residues that are either hexose, deoxyhexose, pentose and hexouronic acid with a respective loss of 162, 146, 132 and 176 amu (Table 3). In contrast, C-type flavonoid glycosides exhibit non-homogenous fragments due to 0,2 and 0,3 cross ring cleavages of the sugar moieties leading to loss of 120 and 90 amu in C-hexosides versus 90 and 60 amu in C-pentosides and 104 and 74 amu in C-deoxyhexosides.

3.3.4. *Flavan-3-ol*

Twenty flavan-3ol, including penylated flavan-3-ol were identified. A few of them were in oligomeric/ polymerized forms (peaks 39, 43, 44, 45, 48, 54, 55, 59, 60, 61, 62, 63, 64, 66, 67, 69, 81, 84, 87, and 103) were identified from the stereoisomers; catechin and epicatechin and from afzelechin (Table 3). The monomers; catechin, epicatechin, gallocatechin and gallo(epi)catechin gave various lengths of polymers called proanthocyanidins (PAs). The two types of *B*-type PAs are linked by C4-C8 or C4–C6 interflavan linkages and *A*-type which have an additional C2–C5 or C2–C7 interflavan ether-linkages between the oligomers. The order of hydrophobicity for flavan-3ol monomers in the reversed-phase liquid chromatography ie (-/+)-epicatechin > (-/+)-catechin > (-/+)-epigallocatechin > (-/+)-gallocatechin also enabled identification of the monomers and the oligoners. The order of elution from the column is in the opposite direction. Thus (-/+)-gallocatechin elutes earlier and epicatechin comes out last. Therefore, (+)-gallocatechin (peaks; 39 and 81), (-)-epigallocatechin (peaks; 43, 44 and 103), (+)-catechin (peak 54) and (-)-epicatechin (peak 55) could be identified. Catechin and epicatechin exhibit fragments *m/z* 151, 135 (due to retro Diels Alder (RDA) fragmentation) upon collision induced dissociation (CID) of their precursor ions $[M\text{-}H]^-$; *m/z* 289. In addition, fragment ions *m/z* 245 ($[\text{catechin -H-44}]^-$, loss of CO_2), *m/z* 205 ($[\text{catechin -H-84}]^-$, loss of flavonoid A ring) and *m/z* 179 ($[\text{M-H-110}]^-$, loss of flavonoid B ring) were consistent with that of the standards' mass spectra and literature (Escobar-Avello et al., 2019). Some polymers of PAs such as (epi)catechin-(epi)gallocatechin gallate (ECEGCG) (peak 61), (epi)gallocatechin-3′-Ogalloyl-(epi)gallocatechin (EGC-OG-EGC) (peak 62) and (epi) gallocatechin-(epi)catechin-(epi)catechin-(epi)catechin (peak 69), (epi) catechin-(epi)catechin -afzelechin-catechin (peak 84) and B-type procyanidin tetramer (peak 87) were formed from the interflavan linkages between different monomers. Peaks 45 and 48 displayed deprotonated molecular ion *m/z* 525 ($[M\text{-}H]^-$), and tentatively identified as derivatives of epicatechin precisely (epi)catechin C-hexoside α-methyl carboxylic acid from the fragments; *m/z* 305 ($[(\text{epi})\text{catechin} -H + 14]^-$, i.e. methyl alkyl group), 451 ((epi)catechin C-hexoside), 246 ([(epi)

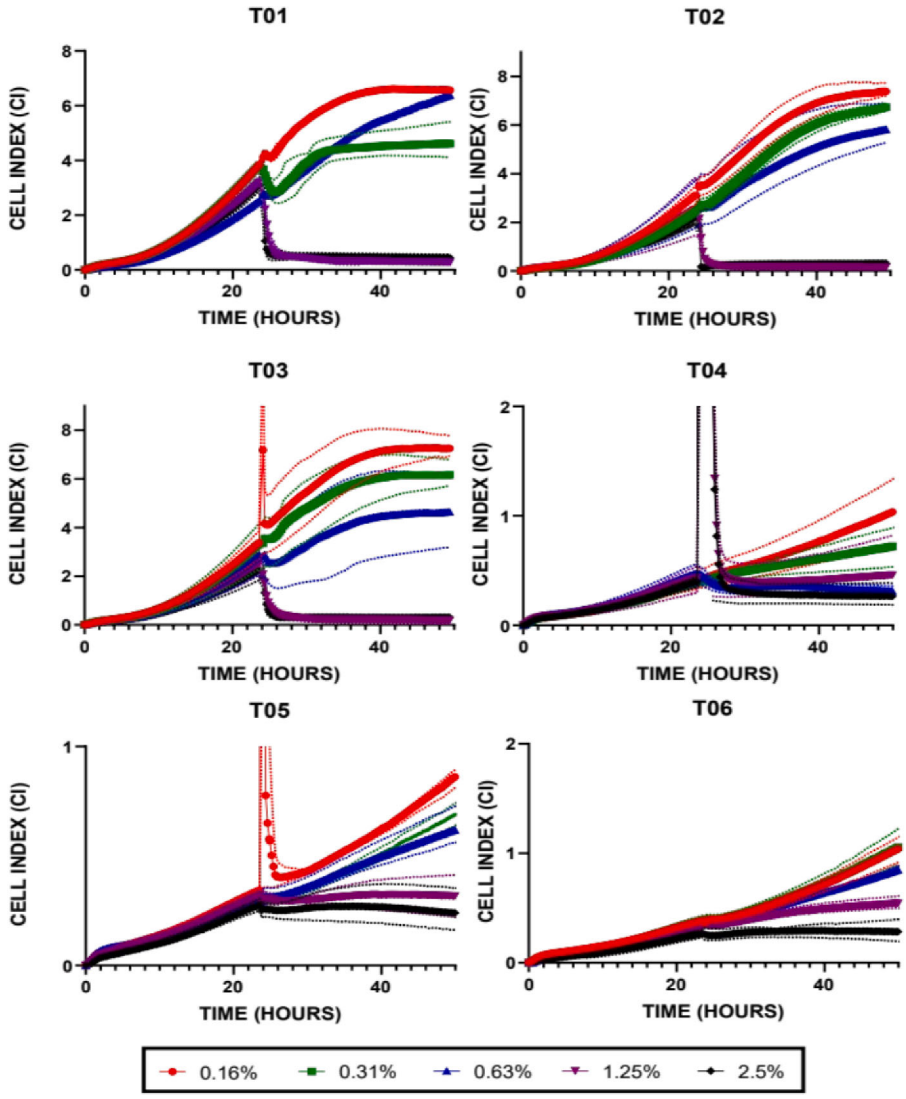

Fig. 3. Cell index vs time post dose calculated using the sigmoidal dose response.

Table 2
Relative toxicity of fractions as determined using xCELLigence real time cell index and plotting the area-under-curve in a time period (CI/hour) vs extract concentration (%).

S/N	Extracts	IC_{50}	R^2
1	T01	0.78 %	0.94
2	T02	0.65 %	0.98
3	T03	0.46 %	0.96
4	T04	0.32 %	0.94
5	T05	2.45 %	0.24
6	T06	1.38 %	0.99

catechin -H-44]$^-$, 164 ([epicatechin -135 + CH_3]$^-$) where *m/z* 135 is [epicatechin - 152]$^-$. The aromatic carboxylic acid comes from loss of OH and followed by decarbonylation (Δm 28) as indicated by ion at *m/z* 479 of the (epi)catechin C-hexoside (451 Da). The diacetyl-(epi)gallocatechin derivative was detected at peak 60. Several prenylated flavon-3-ol oligomers with akyl and alkenyl fragment series were detected in both positive and negative ion modes. Such as (epi)gallocatechin-3′-Ogalloyl-(epi)gallocatechin derivative (alkyl fragment, butyl) (peak 59), (epi)gallocatechin-3′-Ogalloyl-(epi)gallocatechin derivative (alkyl fragment, pentyl) (peak 63 and 66), (epi)catechin-(epi) gallocatechin derivative (alkenyl fragment, butenyl) (peak 67). The alkyl and alkenyl residues could be predicted from the formular C_nH_{2n-1} and C_nH_{2n+1}, (*m/z* 43, 57, 71 …and *m/z* 44, 58, 72 …) respectively (Pretsch et al., 2009). Proanthocyanidins have increasingly been growing linked to plant defense potential, organoleptic characteristics, and potential health benefits through stabilizing the organoleptic properties and color and contributing to the astringency and bitterness (Li and Deinzer, 2009; Rauf et al., 2019). The oligomers of catechin and epicatechin provide protection against predation in plants.

3.3.5. *Flavonols*

Flavonols showed UV strong absorptions at 258 and 348 nm. Nine peaks were identified to belong to those of the flavonols (peaks: 42, 49, 50, 51, 52, 90, 93, 109 and 111) in the extracts. Peak 42 was identified as fistin or 3,7,3′,4′-tetrahydroxyflavone, a plant flavonol with a characteristic ion *m/z* 149 (Table 3). Peaks 49 and 109 was identified as myricetin-3-O-glucoside with the characteristic myricetin aglycone ion 187, 301, 279 identified at peak 111. Peaks 90 and 93 differed by 162 Da (hexoside unit) and were identified dihydroquercetin and dihydroquercetin hexoside respectively due to the sugar conjugation sugar conjugation. The main aglycone ion at *m/z* 305 exhibited fragments; *m/z* 299 and 300 [quercetin -H]$^-$, 153 [$^{1,3}A^+$], formed through retro-cyclization cleavages of the C-ring of the aglycone involving 1 and 3 bond (bonds 1 and 3 refer to the O-C-2 and C-3-C-4 bonds of the C-ring),

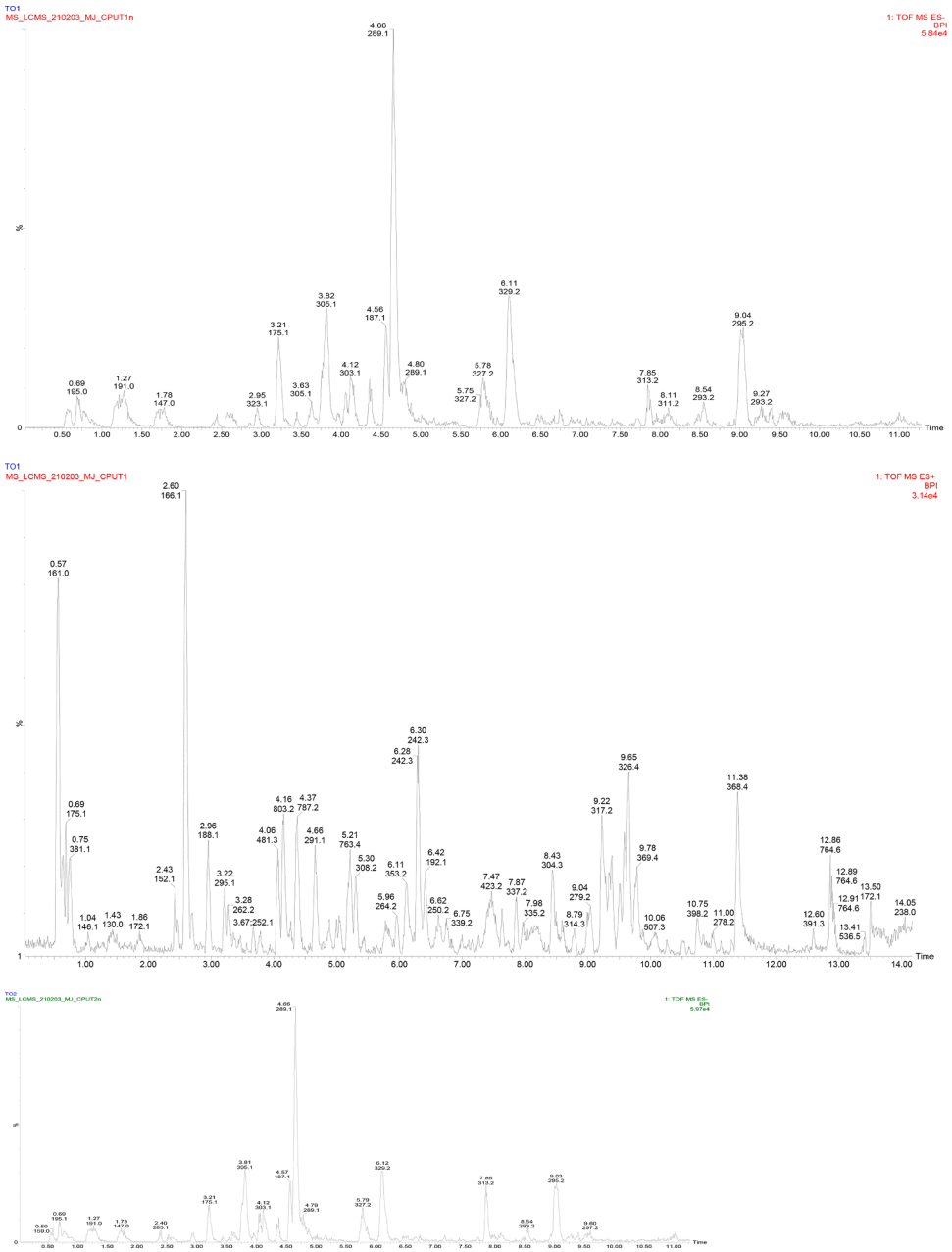

Fig. 4. UHPLC-ESI-MS base peak chromatogram 70 % ethanol of extracts of *T. portulacastrum* cultivars analysed in the ESI negative and ESI positive modes, T01 = *T. portulacastrum* shoot (white flower), T02 = *T. portulacastrum* shoot (purple flower), T03 = *T. portulacastrum* whole plant (white flower), T04 = *T. portulacastrum* whole plant (purple flower), T05 = *T. portulacastrum* root (white flowered), T06 = *T. portulacastrum* root (purple flower).

and 287 $[M\text{-}H\text{-}H_2O]^-$ (Tsimogiannis and Oreopoulou, 2007). Peak 51 displayed ions *m/z* 303, 217, 525, 347 and 479. The strong peak at *m/z* 217 belongs to RDA cleavage of the A ring leading to loss of *m/z* 584 in negative ion mode. The ion at *m/z* 771, was due to loss of CH_3O^- (31 Da) from the glucose molecule on the sophoroside. The *m/z* 449 was due to loss of sophoroside. While thefragment ion *m/z* 303 represents that of the dihyroquercetin. In positive ion mode the parent ion underwent neutral loss of the glucuronide to generate ion *m/z* 177. The ion *m/z* 287 is due to cleavage of C ring in positive ion mode, *m/z* 303 is quercetin in positive ion mode after loss of the sugars. This peak was tentatively identified as quercetin-7-glucuronyl- 3-sophoroside from Metlin data base. Peak 52 with precursor ion $[M-H]^-$ ion; 785.2 fragmented into *m/z* 755, 653, 609, 285, 284, 305, 361, 157 consisted with kaempferol-3-O-sophoroside-7-O-glucuronide from database search (Metlin; http://metlin.scripps.edu/index.php). The CID spectrum of the *m/z* 285 ion, ($[M-H]^-$ ion) originating from heterolytic cleavage of the O-glycosidic bond, consistent with kaempferol. The ion *m/z* 609 was due to the lose glucuronide (176 Da).

3.3.6. *Flavones*

Two flavone peaks were detected and characterised (peaks 38 and 100). UV spectrum, maxima at 269, 344 and 258 nm is characteristic for flavones, with two hydroxyl groups at the ring B. Peak 38 having *m/z* 284, was identified as luteolin. The MS^2 fragments 285 (Metlin; http://metlin.scripps.edu/index.php). Compound 100 was tentatively identified as 2^1,5-Dihydroxy-7-methoxy-6,8-dimethylflavone in line with database search (Metlin; http://metlin.scripps.edu/index.php) and mass match was consistent with earlier reports (Abuzaid et al., 2020)

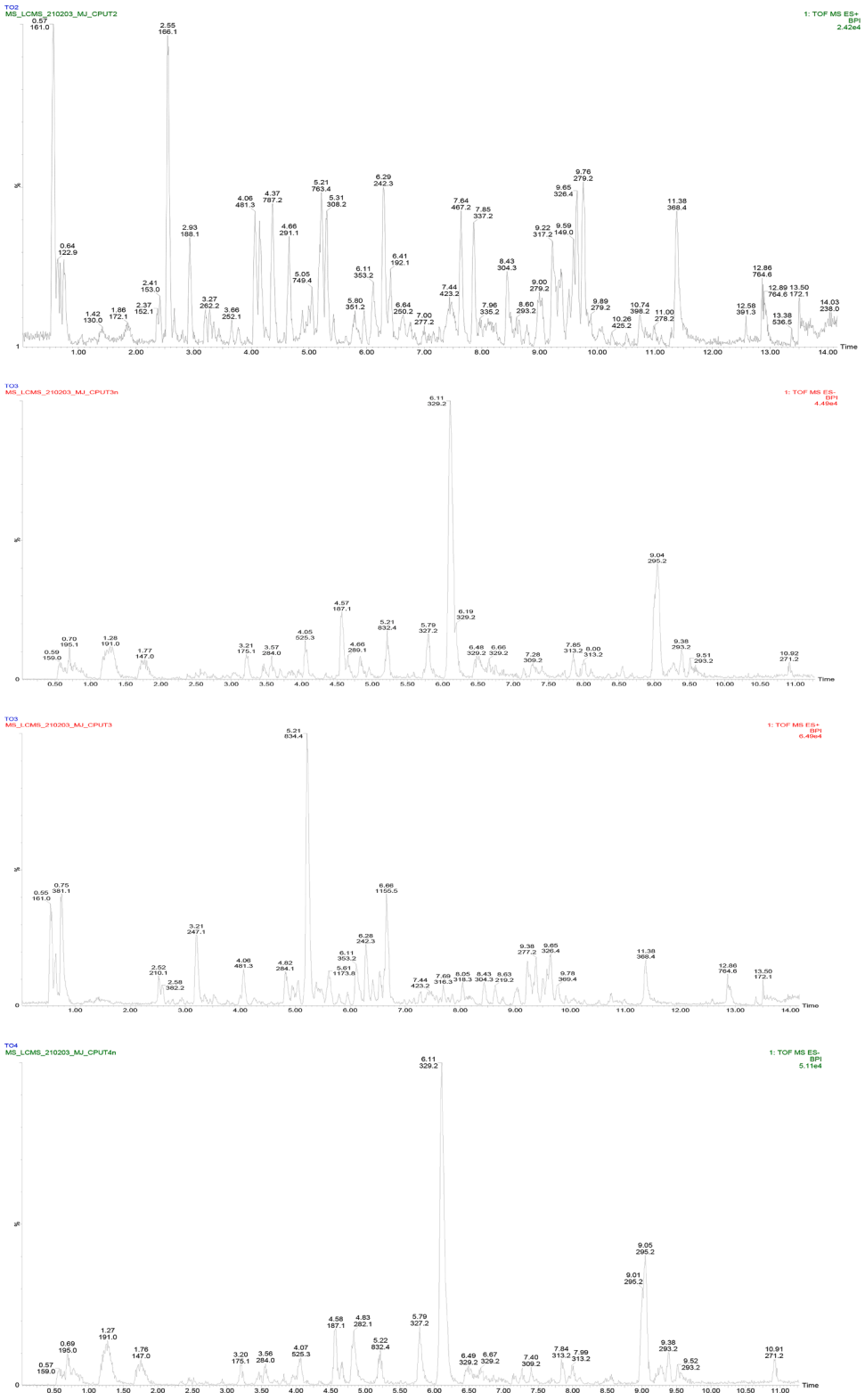

Fig. 4. (*continued*).

3.3.7. *Identification of alkaloids*

Peaks 26, 28, 56, 57, 68, 79, 80 and 98 were identified as those of compounds belonging to alkaloids. Compounds 26 and 68 generated an $[M+H]^+$ ion at *m/z* 247.1434, and it further produced fragment ions at *m/z* 188.0701 $[M+H–NCH_3]^+$ and 146.0598 $[M+H–NCH_3–CO_2]^+$ in the MS^2 spectrum. It was unambiguously identified as hypaphorine, in comparison with literature. Compound 28 was identified as an alkaloid of carboxylic acid. Compound 26 showed a $[M+H]^+$ ion at *m/z* 188.0700. The MS^2 fragment at *m/z* 146 was due to $[M+H–CO_2]^+$ and *m/z* 118 $[M+H–C_2H_2COOH]^+$ and was tentatively identified as *trans*-3-indoleacrylic acid which is consistent with the literature (Harnly et al., 2007). Compound 56and 98, were tentatively identified as N-trans--coumaroyl-tyramine andand N-cis-coumaroyl-tyramine respectively in both positive and negative ion modes. It showed $[M–H]^-$ at *m/z* 282

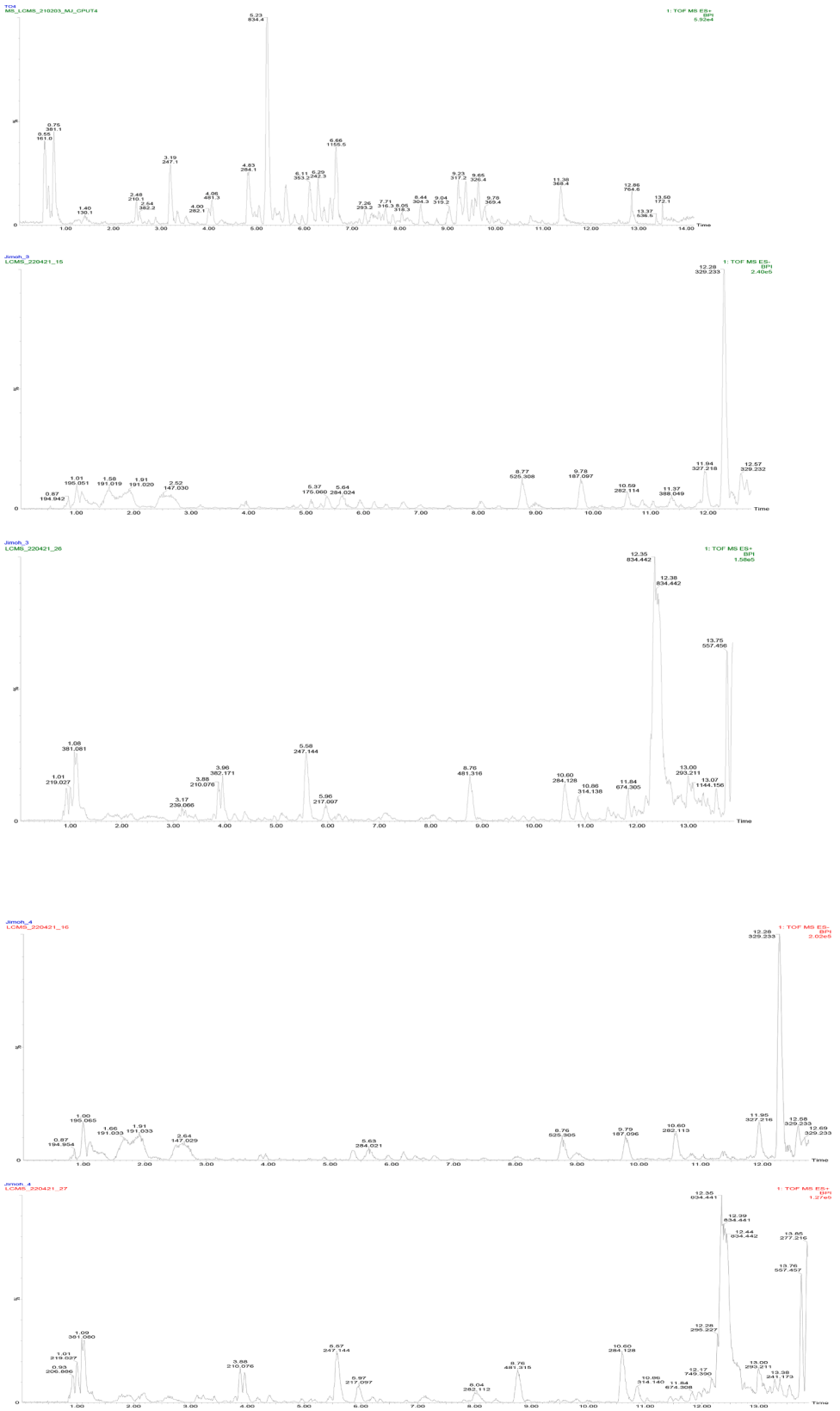

Fig. 4. (*continued*).

and major MS^2 fragments *m/z* 119 ([coumaric acid - CO_2]$^-$ and *m/z* 173 [M−H- coumaric acid -CO_2]$^-$. Compound 57, was identified as *N*-trans-feruloyl-tyramine with $[M+H]^+$ ion at *m/z* 314 and *m/z* 177 [M+H- tyramine]$^+$, 147 [M+H- tyramine-2CH_3]$^+$. Compound 79 was spotted as a breakdown product of ribalinine i.e. dehydrated ribalinine metabolite, after loss of water to give ion *m/z* 242 and other ions *m/z* 149, which is possibly due to ring cleavage from the protoberberine skeleton (Deevanhxay et al., 2009) and *m/z* 177 MS^2 fragment *m/z* 177

Table 3
Qualitative analysis of compounds from *T. portulacastrum*.

No	t_R (min)	MF	UVλ_{max} (nm)	*m/z* $(M-H)^-$ / $(M+H)^+$	MS/MS	Tentative identification	Sample
1[b]	0.60	$C_{10}H_8O_2$	267	158.9767	115	Methylcoumarin	T1, T2, T3, T4
	0.60	$C_{10}H_8O_2$	267	161.0294*	147	Methylcoumarin	T1, T3, T4
2[b]	0.62	$C_{10}H_8O_2$	267	161.0296*	147	Methylcoumarin	T3
3[b]	0.63	$C_{11}H_{10}O_4$	267	206.8863*	123, 191	Limettin (dimethoxycoumarin)	T2, T3, T4
4[b]	0.70	$C_6H_{12}O_7$	267	195.0490	174, 165, 147, 129, 135, 132	Gluconic/ galactonic acid	T1, T2, T3, T4, T5, T6
5[b]	0.70	$C_{11}H_{10}O_2$	267	175.1192*	161, 140	Dimethyl coumarin	T1, T2, T3, T4
6[b]	0.75	$C_{17}H_{16}O_9$		381.0798**	144, 249, 365, 175, 188, 365, 162, 174, 145	Xanthotoxol-glucoside	T1, T2, T3, T5, T6
7[b]	0.87	$C_{10}H_{10}O_4$		195.0513	177	Isoferulic acid/Dihydroferulic acid	T5, T6
8[b]	0.90	$C_{22}H_{20}O_8$		414.8839*	317, 219, 167, 349, 137	Limettin dimer	T6
9[b]	0.93	$C_{11}H_{10}O_4$		206.8860*	123, 140, 191	Limettin	T6
10[b]	1.01	$C_{12}H_{10}O_4$		219.0269**^{H2}	175, 203, 189, 156	Ethoxy- methoxy coumarin	T5, T6
11[b]	1.04	$C_9H_6O_2$		146.0923*	130, 136	Coumarin	T1, T2
12[b]	1.30	$C_6H_7O_7$	262	191.0186	173, 111, 87	Citric acid	T1, T2, T3, T4, T5, T6
13	1.40	–		130.0507*	130	Unknown	T2
14	1.80	$C_5H_8O_5$	262	147.0283	87, 125, 110	Unknown	T1, T2, T3, T4
15[b]	1.90	$C_5H_8O_5$		172.1189^{Na}	149, 132	Coumarin	T2
16[b]	2.40	$C_{12}H_{12}O_8$	271, 330	283.0638	151, 227, 209, 142	dihydroxy benzoic acid derivative	T1, T2
17[b]	2.40	$C_7H_5O_4$	264, 330	153.0565*	137	Protocatechuic acid	T1, T2
18[b]	2.40	$C_{21}H_{19}O_7$	273	383.1300	323, 282, 341, 200, 188, 161	1,3-O-Dicoumaroylglycerol	T3
19[b]	2.50	$C_{11}H_8O_5$	273	210.0761 ^{Li}	164, 192, 144, 149	Glucaric acid	T3, T5, T6
	2.50		273	208.0589	142, 191, 173, 161	Glucaric acid	T3
20	2.52	$C_5H_8O_5$		147.0285	129	Citramalate	T5, T6
21[b]	2.60	$C_{19}H_{18}O_4$	268	309.1221	164, 230, 119, 134, 153, 193	p-Coumaric acid deoxyhexose	T1, T2
22[a]	2.60	$C_9H_{11}NO_2$	268	166.0863*	120	L -Phenylalanine	T1
23[b]	2.60	$C_{10}H_{13}O_2$	264	161.0533	101	Saccharide	T2
24[b]	2.60	$C_{24}H_{29}O_4$	267	380.1555	309, 203, 241, 321	p-Coumaric acid deoxyhexose derivative	T3, T5, T6
	2.60	$C_{24}H_{29}O_4$	267	382.1704*	220, 166, 210, 247, 120, 149, 182	p-Coumaric acid deoxyhexose derivative	T3, T4, T5, T6
25[b]	2.70	$C_{11}H_8O_5$	268	220.1170**	195, 120, 149	Xanthotoxol	T1, T2
26[b]	2.96	$C_{14}H_{18}O_2N_2$	268	247.1442*	188, 146, 149	Hypaphorine	T3, T4
27[b]	3.00	$C_{15}H_{17}O_8$	268	323.1307 (325)	179, 119, 89, 149, 161, 151, 204	Phenylpropenoic acid glucoside (PPAG)	T1, T2
28[b]	3.10	$C_{14}H_{18}O_2N$	268	188.0705*	146, 149	Trans-3-indoleacrylic acid	T1, T2
29[b]	3.10	$C_{22}H_{22}O_8$	270	414.1057	403, 136, 109, 179, 208	1,3-O-Coumaroyl-feruloylglycerol	T3
30[b]	3.17	$C_{12}H_8O_4$		239.0663^{Na}	132, 229, 205, 190, 172, 144	Xanthotoxin	T5
31[b]	3.19	$C_{14}H_{14}O_5$	266	263.1385*	220, 184, 174, 149	Leptophyllin	T6
32[b]	3.20	$C_{13}H_{12}O_8$	260	295.1299*	174, 149	Coumarin derivative	T1, T2
33[b]	3.22	$C_6H_8O_6$	260	175.0600	115, 85	L-(+)-ascorbic acid	T1, T2, T3, T4
34[b]	3.30	$C_{14}H_{14}O_5$	260	262.1637*	149, 177	Diacetyl methoxycoumarin	T1, T2
35[b]	3.34	$C_{12}H_8O_4$		217.0981*	144, 149, 177, 164	Xanthotoxin	T2
36[b]	3.50	$C_{26}H_{30}O_{11}$	289, 325	517.1871	403, 236, 433, 375, 192, 165	1,3-O-Coumaroyl-feruloylglycerol derivative	T2
37[b]	3.50	$C_{11}H_9O_6$	267	236.0559	209, 191	Glucaric acid derivative	T3, T4
38[b]	3.60	$C_{15}H_9O_6$	279	284.0209	204, 193, 157	Luteolin	T3, T4
39[b]	3.63	$C_{15}H_{14}O_7$	267, 323	305.1063	305, 157, 250, 203, 275, 285, 115, 164	(-/+)Gallocatechin	T1, T2, T3, T4
40[b]	3.70	$C_9H_8O_3$	267	165.0183	121, 130	Acetyl-4-hydroxybenzaldehyde	T3
41[b]	3.70	$C_{12}H_8O_5$		252.0871**	134, 149, 177, 234	5-Methoxy-8-hydroxypsoralen	T2
42[b]	3.80	$C_{15}H_{10}O_6$	268, 315	287.0541*	177, 149, 105	Fisetin (3,7,3′,4′-tetrahydroxyflavone)	T1, T2
43[b]	3.80	$C_{15}H_{14}O_7$	265, 335	305.1046	186, 195, 275	(-/+) (Epi)gallocatechin	T2
44[b]	3.82	$C_{15}H_{14}O_7$	268, 315	305.1053	97, 297, 164, 284, 115, 158, 221	(-/-) (Epi)gallocatechin	T1, T2
45[b]	4.00	$C_{25}H_{50}O_{11}$	319	525.3035	305, 479, 515, 451, 246, 164	(epi)catechin C-hexoside α-methyl carboxylic acids	T2, T5, T6
46[b]	4.00	$C_{10}H_6O_3$	275, 308	173.0826	164, 123	Coumarin derivative	T3
47[b]	4.00	$C_{16}H_{11}O_6$	275, 308	282.1112^{Na}	177, 147, 149, 203	Acetyl xanthotoxin	T3, T4
48[b]	4.10	$C_{24}H_{46}O_{12}$	323	525.3034	305, 303, 192, 479, 451, 246, 164, 205	(Epi)catechin C-hexoside α-methyl carboxylic acids	T1, T3, T5, T6
49[b]	4.10	$C_{21}H_{20}O_{12}$	323	481.3145*	463, 445, 371, 266, 149, 427, 303	Myricetin-3-O-glucoside	T1, T2, T3, T4, T6
50[b]	4.12	$C_{15}H_{11}O_7$	323	303.0901	97, 217, 206, 164	Dihydroquercetin (taxifolin)	T1, T2
51[b]	4.20	$C_{33}H_{38}O_{23}$	340	801.1877	303, 217, 771, 477	Quercetin-7-O-glucuronyl-3-O-sophoroside	T1, T2
	4.20	$C_{33}H_{40}O_{23}$	340	803.2045*	303, 339, 177, 287	Quercetin-7-O-glucuronyl-3-O-sophoroside	T1, T2
52[b]	4.40	$C_{33}H_{38}O_{22}$	266, 326	785.1934	755, 653, 609, 285, 284, 305, 361, 157	Kaempferol-3-O-sophoroside-7-O-glucuronide	T1, T2
	4.40	$C_{33}H_{40}O_{22}$	266, 326	787.2068*	287, 757, 197, 245, 177, 339, 149	Kaempferol-3-O-sophoroside-7-O-glucuronide	T1, T2
53[b]	4.56	$C_7H_8O_6$	268, 280, 316	187.0974	125, 169	Gallic acid monohydrate	T1, T2, T3, T4, T5, T6
54[a]	4.66	$C_{15}H_{14}O_6$	268	289.1096	289, 97	Catechin	T1, T2, T3, T4
55[a]	4.73	$C_{15}H_{14}O_6$	234, 280	289.1104	289, 243	Epicatechin	T1, T2
	4.73	$C_{15}H_{14}O_6$	234, 280	291.1267*	193, 227, 215	Epicatechin	T1, T2
56[b]	4.80	$C_{17}H_{17}NO$	283, 309	282.1102	119, 187, 173	N-trans-Coumaroyl-tyramine	T3, T4, T5, T6
	4.80	$C_{17}H_{17}NO_3$	283, 309	284.1273*	147, 177, 149, 121	N-trans-Coumaroyl-tyramine	T3, T4, T5, T6
57[b]	4.90	$C_{18}H_{19}NO_4$	288, 309	312.1248	282, 173, 187	N-trans-Feruloyl-tyramine	T3

(*continued on next page*)

Table 3 (*continued*)

No	t_R (min)	MF	UVλ_{max} (nm)	*m/z* $(M-H)^-$ / $(M+H)^+$	MS/MS	Tentative identification	Sample
	4.90	$C_{18}H_{19}NO_4$	288, 309	314.1386*	284, 171, 186, 149, 177	N-trans-Feruloyl-tyramine	T3, T4
58[b]	4.90	$C_{13}H_{14}O_6$		267.1205*	209, 191, 171	Glucaric acid derivative	T1, T2
59[b]	5.00	$C_{41}H_{38}O_{18}$	288	820.4205*	291, 309, 367, 275, 258, 351, 149, 725	(Epi)gallocatechin-3′-Ogalloyl- (epi)gallocatechin derivative(alkyl fragment, butyl)	T1, T2
60[c]	5.03	$C_{19}H_{17}O_9$	280	388.0491	222, 345, 301, 266	Diacetyl-(epi)gallocatechin	T5, T6
61[b]	5.10	$C_{36}H_{40}O_{18}$		749.3853*	309, 367, 275, 149, 177, 293	(Epi)catechin-(epi)gallocatechin gallate (ECEGCG)	T1, T2, T3, T4, T6
62[b]	5.20	$C_{37}H_{30}O_{18}$		763.4038**	367, 309, 149, 177, 291, 251 144, 146, 192, 304, 326, 369, 398, 487, 677	(Epi)gallocatechin-3′-Ogalloyl- (epi)gallocatechin (EGC-OG-EGC)	T1, T2, T3, T4, T5, T6
63[c]	5.20	$C_{43}H_{29}O_{18}$	276	832.4186	761, 807, 201, 289, 241, 301, 343, 193, 183	(Epi)gallocatechin-3′-Ogalloyl- (epi)gallocatechin derivative(alkyl fragment, pentyl)	T1, T2, T3, T4, T5, T6
	5.20	$C_{43}H_{29}O_{18}$	276	834.4382**	721, 392, 174, 86, 580, 664, 203, 336, 307, 763, 269, 410	(Epi)gallocatechin-3′-Ogalloyl- (epi)gallocatechin derivative (alkyl fragment, pentyl)	T1, T2, T3, T4, T5, T6
64[c]	5.30	$C_{19}H_{14}O_4$		308.2210*	177, 149, 257	(Epi)gallocatechin isomer	T1, T2
65[b]	5.37	$C_6H_8O_6$		175.0592	157	Ascorbic acid	T5, T6
66[c]	5.40	$C_{43}H_{29}O_{18}$		834.4407*	650, 625, 149, 177, 721	(Epi)gallocatechin-3′-Ogalloyl- (epi)gallocatechin derivative (alkyl fragment, pentyl)	T3, T5
67[c]	5.50	$C_{28}H_{25}O_{18}$		650.3541*	625, 389, 301, 149, 203, 177, 367, 643	(Epi)catechin-(epi)gallocatechin derivative (alkenyl fragment, butenyl)	T3, T4
68[b]	5.58	$C_{14}H_{18}O_2N_2$		247.1442*	188	Hypaphorine	T5, T6
69[b]	5.60	$C_{60}H_{52}O_{25}$		1173.7850*	674, 880, 777, 217, 365	(Epi)gallocatechin-(epi)catechin-(epi)catechin-(epi)catechin	T3, T4
70[b]	5.64		278	284.0207	186, 142, 209	Unknown, luteolin?	T5, T6
71[b]	5.78	$C_{18}H_{32}O_5$		327.2167	229, 171, 145, 183, 239, 211	oxo-dihydroxy-octadecenoic acid	T1, T3, T4, T5, T6
72[b]	5.81	$C_{17}H_{18}O_7$		351.2147**	293, 275, 195, 149	Byakangelicin	T1, T2, T3, T4
73[b]	5.96	$C_{12}H_8O_4$		217.0977*	144	Xanthotoxin	T5, T6
74[b]	6.00	$C_{14}H_{14}O_5$		264.2318*	219, 226	Leptophyllin	T1, T2, T3, T4
75[b]	6.00	$C_{12}H_{12}O_5$	275	236.0551	192, 215, 174	Unknown	T5, T6
76[b]	6.11	$C_{18}H_{34}O_5$		329.2325	229, 211, 171, 183, 139, 127	Trihydroxy-octadecadienoic acid	T1, T3, T4
77[b]	6.11	$C_{18}H_{34}O_5$		353.2304^{Na}	295, 195, 120	Trihydroxy-octadecadienoic acid	T1, T2, T3, T4
78[b]	6.20	$C_{10}H_9O_5$	274	209.0432	191, 157	Glucaric acid	T5, T6
79[b]	6.30	$C_8H_{10}O_8N$	274	242.2842*	149, 177	Dehydrated ribalinine	T1, T2, T3, T4
80[b]	6.40	$C_{11}H_{13}NO_2$	274	192.1385*	181, 149, 177	3,4-dihydro-6,7-dimethoxy- isoquinoline	T1, T2, T3
81[b]	6.40	$C_{15}H_{14}O_7$		305.1135	195, 255, 215	Gallocatechin	T6
82[b]	6.50	$C_{14}H_{17}O_9$		329.2361	329, 309, 307, 197, 171, 128	Ethylgallate pentoside	T1
83[b]	6.50	$C_{18}H_{34}O_5$		329.2326	229, 211, 173,	Trihydroxy-octadecadienoic acid	T3, T4, T5, T6
84[b]	6.50	$C_{60}H_{55}O_{23}$		1144.1564*	353, 245, 120, 149, 387, 291, 293, 650, 277, 293, 563, 417	(Epi)catechin-(epi)catechin -afzelechin-catechin	T3, T4, T5
85[b]	6.62	$C_{12}H_8O_5$		250.1783**	228	5-Methoxy-8-hydroxypsoralen	T1
86[b]	6.66	$C_{18}H_{34}O_5$		329.2318	229, 211, 167, 144	Trihydroxy-octadecadienoic acid	T3, T4, T5
87[b]	6.66	$C_{60}H_{50}O_{24}$		1155.5150*	862, 353, 250, 149, 227, 881	B-type procyanidin tetramer ((Epi)catechin-(*epi*)catechin-(*epi*)catechin-(*epi*)catechin)	T3, T4
88[b]	6.80	$C_{17}H_{16}O_6$		339.1771^{Na}	291, 225, 299	Apaensin	T1
89[b]	6.80	$C_{18}H_{34}O_4$		315.1784	307, 187, 235, 211, 145, 128	Dihydroxy-octadecadienoic acid II	T1, T2
90[b]	7.20	$C_{15}H_{11}O_7$		305.1736	299, 300, 153, 265, 287	Dihydroquercetin	T3
91[b]	7.30	$C_{18}H_{29}O_4$		309.2042	283, 284, 209, 185, 171	Linoleic acid hydroperoxide isomer	T3, T4
92[b]	7.40	$C_{21}H_{24}O_9$		423.2357*	398, 337, 149, 279, 383	Diacetyl byakangelicin	T1, T2
93[b]	7.60	$C_{21}H_{22}O_{12}$		467.1950*	445, 423, 277, 225, 183	Dihydroquercetin hexoside	T1, T2, T4
94[b]	7.70	$C_{18}H_{30}O_3$		316.2853^{Na}	149, 239	Hydroxylinolenic acid	T3
95[b]	7.85	$C_{18}H_{32}O_4$		313.2358	183, 169, 128, 99, 223, 295, 307	Dihydroxy octadecenoic acid II	T1, T2, T3, T4
	7.90	$C_{18}H_{32}O_4$		337.2324*	319, 209, 119, 299	Acetoxy-6-gingerol	T1, T2
96[b]	8.00	$C_{18}H_{32}O_4$		335.2188*	307, 295, 288, 277, 177, 149	Acetoxy-6-gingerol	T1, T2
	8.00	$C_{18}H_{32}O_4$		313.2363	307, 201, 209, 187	Dihydroxy octadecenoic acid I	T3, T4
97[b]	8.00	$C_{18}H_{32}O_3$		318.2997^{Na}	307, 149	Hydroxy-octadecadienoic acid	T3, T4
98[b]	8.04	$C_{16}H_{11}O_6$		282.1122^{Na}	147, 217	N-cis-Coumaroyl-tyramine	T6
99[b]	8.08	$C_{17}H_{18}O_7$		674.3054*	498, 203, 177, 509	Byakangelicin isomer II dimer	T5, T6
100[b]	8.10	$C_{18}H_{16}O_5$		311.1678	283, 221, 265	2^1,5-Dihydroxy-7-methoxy-6,8-dimethylflavone	T3, T5, T6
101[b]	8.10		291	429.1423	280, 298	1,3-O-Feruloyl-caffeoylglycerol	T5, T6
102[b]	8.11	$C_{18}H_{30}O_4$		311.2207	311, 291, 187	Dihydroxy-octadecadienoic acid	T1, T2, T5
103[b]	8.20	$C_{15}H_{14}O_7$		307.1872*	149, 242, 177, 229	(-)-Epigallocatechin	T2, T3, T4
104[b]	8.40	$C_{19}H_{30}O_3$		304.2992*	277, 149, 177	Hydroxy linolenic acid derivative	T1, T2, T3, T4
105[b]	8.54	$C_{18}H_{32}O_3$		293.2098	128, 224, 271	Hydroxy-octadecadienoic acid	T2
106[b]	8.54	$C_{18}H_{30}O_3$		293.2096**	277, 177, 149	Hydroxylinolenic acid	T1
107[b]	8.60	$C_{18}H_{34}O_5$		315.2504	271, 311	Dihydroxy-octadecadienoic acid derivative	T3, T4
108[b]	8.60	$C_{12}H_{10}O_4$		219.1754*	149, 177, 200	Ethoxy- methoxy coumarin	T3, T4
109[b]	8.76	$C_{21}H_{20}O_{12}$		481.3154*	445, 463, 347, 427, 303, 371	Myricetin-3-O-glucoside	T5, T6
110[b]	8.80	$C_{18}H_{32}O_4$		314.2859^{Na}	293, 149, 177	Hydroxy-octadecadienoic acid II	T1, T2, T5, T6
111[b]	9.00	$C_{15}H_{10}O_8$		319.2254*	187, 301, 279	Myricetin	T3, T4
112[b]	9.04	$C_{18}H_{32}O_3$		295.2259	277, 195, 171, 150, 221, 265	Hydroxy octadecadienoic acid	T1, T2, T3, T4, T5, T6
113[b]	9.20	$C_{18}H_{32}O_3$		317.2081^{Na}	277, 177, 149, 135, 185, 301, 205	Hydroxy octadecadienoic acid	T1, T2, T3, T4
114[b]	9.27	$C_{18}H_{30}O_3$		293.2110	265, 128	Hydroxy octadecadienoic acid isomer 2	T1, T3, T4
115[b]	9.30	$C_{27}H_{16}O_5$		421.2321*	277, 399, 317, 295, 332, 335, 149	Hydroxy octadecadienoic acid derivative	T1, T2

(*continued on next page*)

Table 3 (*continued*)

No	t_R (min)	MF	UVλ_{max} (nm)	*m/z* $(M-H)^-$ / $(M+H)^+$	MS/MS	Tentative identification	Sample
116[b]	9.30	$C_{18}H_{30}O_3$		293.2086	265, 187, 128, 230	Hydroxy-octadecadienoic acid I	T4
117[b]	9.38	$C_{18}H_{30}O_3$		293.2106	265, 196, 128	Hydroxy-octadecadienoic acid II	T4
118[b]	9.52	$C_{18}H_{30}O_3$		293.2120	265, 128	Hydroxy-octadecadienoic acid II	T4
119[b]	9.40	$C_{17}H_{16}O_6$		317.2085^{Na}	119, 179	Byakangelicol	T3, T4
120[b]	9.40	$C_{18}H_{30}O_2$		277.2157*	149, 179	Linolenic acid isomer	T1, T2, T6
121[b]	9.50	$C_{18}H_{17}O_2$		265.1479	265, 247, 245	Magnolol	T1
122[b]	9.50	$C_{18}H_{32}O_3$		317.2092^{Na}	277, 179, 149, 135, 185	Hydroxylinolenic acid	T1, T2, T3, T4
123[b]	9.61	$C_{18}H_{30}O_3$		295.2269*	277, 149, 195, 177	Hydroxylinolenic acid	T6
124[b]	9.67	$C_{18}H_{30}O_3$		293.2113*	275, 177, 149, 192	Hydroxylinolenic acid isomer	T6
125[b]	9.70	$C_{17}H_{16}O_5$		326.3781^{Na}	301, 149, 205, 177, 186, 133, 121	Phelloptorin	T1, T2, T3, T4
126[b]	9.75	$C_{18}H_{30}O_2$		557.4565*	279, 521	Linolenic acid dimer	T5, T6
127[b]	9.78	$C_{15}H_{30}O_2$		241.1735*	225, 195, 149	pentadecanoic acid	T6
128[b]	9.80	$C_{21}H_{20}O_6$		369.3849*	279, 338, 149, 297, 319	Isoglycycoumarin	T1, T2, T3, T4
129[b]	10.90	$C_{17}H_{32}O_3$		271.2273	128	hydroxy-palmitic acid	T3, T4
130[b]	11.00	$C_{28}H_{43}O_{11}$		555.2793	353, 311, 327, 265, 150	Picrasinoside F	T1, T2
131[b]	11.40	$C_{22}H_{20}O_6$		379.1553	279, 311, 325, 265, 353	Unknown	T1, T2
132[b]	11.40	$C_{21}H_{20}O_6$		368.4246*	325, 181, 109, 149, 299	Isoglycycoumarin	T1, T2, T3, T4
133[b]	11.90	$C_{20}H_{20}O_6$		355.1553	325, 340, 279, 196, 265	Piperitol	T1, T2
134[b]	13.50	$C_{12}H_{10}O_4$		248.9572	113, 181, 128	Piperic acid	T1, T2, T3, T4

Results are presented as T1- *T. portulacastrum* shoot (white flower), T2- *T portulacastrum* shoot (purple flower), T3- *T portulacastrum* whole plant (white flower), T4- *T portulacastrum* whole plant (purple flower), T5- *T portulacastrum* root (white flowered), T6- *T portulacastrum* root (purple flower). *M/z* in $(M-H)^-$ = negative ion mode and *$[M+H]^+$, **$[M+NH_4]^+$, $^{Na}[M+Na]^+$ and $^{Li}[M+Li]^+$ for positive ion mode.

[a] Identified using reference standard.

[b] Determined with aid of literature using accurate mass match, reference compound and number of carbon atoms.

[c] Novel compound, In some instances, structural isomers have different retention times but represented by the same general name such as epigallocathechin (it can be (-)-epigallocathechin or (+)-epigallocathechin).

($[192\text{-}CH_3]^+$) from the isoquinoline skeleton ion *m/z* 192 (Chrzanowska et al., 2016; Qing et al., 2015). Compound 80 was tentatively identified as 3,4-dihydro-6,7-dimethoxy- isoquinoline with $[M+H]^+$ ion at *m/z* 192.1385 and major MS^2 fragment ions *m/z* 177$[M+H–CH_3]^+$ and m/z 149$[M+H–CH_3–CO]^+$ (Algharib, 2010; Molnár et al., 2022).

3.3.8. Identification of coumarins and furanocoumarins

Coumarins and furanocoumarins were detected at peaks 1, 2, 5, 6, 7, 8, 9, 10, 11, 15, 25, 30, 31, 32, 34, 35, 41, 46, 47, 72, 73, 74, 85, 88, 92, 99, 108, 119, 125, 128, and 132. Most of which exhibited uv λ_{max} at 274 nm; characteristic of coumarins UV absorptions (Table 3). Peaks 1, 2, 3,5, 7, 8 and 9, belonged to either methyl or hydroxyl, methoxy or ethoxy and dimethoxy derivatives of coumarin through addition of one or more of the 14 or 17or 31 or 45 and 62 mass units to *m/z* 145/147/149 for coumarin respectively. Free coumarin was identified at peaks, 11 and 15. Its acetyl derivative (peak 28) and an unknown coumarin derivative (peak 32, 46 and79) were detected too. Ethoxy- methoxy coumarin derivatives were detected in the extracts TO3, TO4, TO5 and TO6 (peaks 10 and 108). Peak 30, 35 and 73 was tentatively identified as xanthotoxin (hydroxyl psoralen) as a protonated, or sodium adduct in the positive ion mode with MS^2 of characteristic ion, *m/z* 203 for xanthoxol, *m/z* 192 $[M+H–CO]^+$, 177 $[M+H–CO_2]^+$. Its acetyl derivative was identified at peaks 47 and 98. Furthermore, Peak 41 and 85 was proposed to be as 5-methoxy-8-hydroxypsoralen with ammonium adduct ion at *m/z* 252 (Gao and Li, 2023; Li et al., 2014). The MS^2 fragment at *m/z* 234 (for the protonated ion), *m/z* 177 $[M+H–CH_3–CO_2]^+$. Peak 31 and 74 was identified as leptophyllin in accordance with literature. It displayed with $[M+H]^+$; 263 and MS^2 fragments *m/z* 219/220 $[M+H–CO_2]^+$. Byakangelicin was identified as an ammonium adduct in positive ion mode at *m/z* 351, its diacetyl derivative was suggested to have been found in peaks 92 and 99. Byakangelicin gave MS^2 fragment ions at *m/z* 293, 275, 195, 149 (Yang and Li, 2022)

3.3.9. Identification of lignans

Peaks 121, 130 and 133 were identified to belong to those of lignans (Table 3). Piperitol was detected in peak 133 and exhibited major MS/MS fragments; *m/z* 325 ($[M–H–CH_3O]^-$), 340 ($[M–H–CH_3]^-$) and 265 ($[M–H–CH_3O–OH–OCH_2O]^-$). Compound with peaks 121 and 130, were identified to be magnolol and picrasinoside F in accordance with data base search, Metlin (http://metlin.scripps.edu/index.php).

3.3.10. Identification of fatty acids

Next to flavonoids and phenolic acids, fatty acids amounted as the third abundant class in extracts represented by a total of 32 known (71, 76, 77, 83, 86, 89, 91, 94, 95, 96, 97, 100, 102, 104, 105, 106, 107, 110, 112, 113, 114, 115, 116, 117, 118, 120, 122, 123, 124, 126, 127, and 129) fatty acid peaks (Table 3). Characterized fatty acids were predominated by poly unsaturated and hydroxylated forms. Peak 126 was identified as that of linoleic acid dimer and the isomeric at peak 120 and its fragmentation pattern is similar to that from previous work (Serag et al., 2020). Its hydroxylated form was represented at peaks 94, 106, 122, 123, and 124. They showed extra loss of water molecules. They are known to possess antimicrobial and cytotoxic activities (Martin-Arjol et al., 2010). The unknown derivative of linoleic acid could be detected at peak 104. Linoleic acid was ubiquitous in all the tested extracts of *T. portulacastrum*. The polyunsaturated fatty acids included; oxo-dihydroxydecanoic acid at peak 71 and trihydroxy-fatty acid; trihydroxyoctadecadienoic acid (peaks 73, 76, 83 and 86). Trihydroxyoctadecanoic acid showed main MS/MS fragments at *m/z* 311 and 293 due to subsequent loss of two water molecules and a main fragment at *m/z* 211 due to the C15\C16 bond cleavage (Serag et al., 2020; Spínola et al., 2014). Additionally, dihydroxy derivatives of octadecanoic acid, dihydroxyoctadecanoic acid was shown at peak 89, 95, 96, 100, 102 and ite derivative at peak 107. Besides, LC–MS also revealed several monohydroxy-fatty acid peaks including hydroxyoctadecanoic acid and its derivatives. Lastly, the saturated fatty acid, pentadecanoic acid was identified at peak 127 in agreement with previous work (Serag et al., 2020).

3.3.10.1. Identification of amino acids. Peak 22 was identified as phenylalanine, based on a molecular ion peak $[M+H]^+$ at *m/z* 166.0863 (calcd 166.0863). CID of this protonated molecular ion produced a characteristic fragment ion $[M+H–H_2O + CO]^+$ at *m/z* 120.0800 due to the loss of H_2O+CO moieties (46 Da).

Table 4
Limit of detection (LOD) and limit of quantitation (LOQ) values calculated for chemical markers.

No	Name	t_R (min)	$UV_{\lambda max}$ (nm)	*m/z* $(M-H)^-$	*m/z* MS/MS	Regression equation	Linear range mg/L	R^2	LOD mg/L	LOQ mg/L
1	Catechin	8.7	278	289	289, 245, 205, 137, 109	$y = 1163.4x$	3.9–31.3	0.999	1.7	5.8
2	Caffeic acid	9.4	300, 322	179	179, 135	$y = 703.7x + 20.9$	3.9–31.3	1.000	2.9	9.5
3	Epicatechin	10.8	278	289	289, 245, 205, 137, 109	$y = 1553.3x + 938.1$	3.9–31.3	0.998	1.3	4.3
4	p-coumaric acid	11.8	300, 309	163	163, 119	$y = 625.1x - 516.0$	3.9–31.3	1.000	3.2	10.7
5	Ferulic acid	13.4	300, 322	193	193, 179, 149, 134	$y = 487.8x - 57.7$	3.9–31.3	0.997	4.1	13.7
6	Rutin	14.5	254, 255, 354	609	609, 301	$y = 1155.5x + 205.9$	3.9–31.3	0.998	1.7	5.8
7	Hesperidin	17.4	284, 330	609	608, 301	$y = 610.4x + 7.9$	3.9–31.3	0.994	3.3	11.0
8	Phloridzin	17.9	284	435	435, 273, 167	$y = 1308.6x + 1603.3$	3.9–15.6	1.000	1.5	5.1

Flavanols were quantified against catechin and thus expressed as catechin equivalents, flavanones were expressed as hesperidin equivalents, flavonols were expressed as quercetin equivalents, while dihydrochalcones were expressed as phloridzin equivalents.

3.3.10.2. Identification of organic acids. Peaks 4 and 20 were identified to be those of organic acids. Peak 4 identified as that of gluconic/ galactonic acid with parent ion *m/z* 195.0490 and a characteristic MS^2 ion at *m/z* 129 according to earlier reports (Goger et al., 2015). Peak 20 was identified to be that of citramalate using earlier literature (Kappelmann et al., 2017).

3.3.11. HPLC DAD and UPLC-QTOF-Ms quantitation of phenolic compounds

The primary means of quantifying phenolic compounds is UV/vis absorption and, as stated earlier, this can be used to distinguish the different phenolic subclasses. Based on the qualitative analysis, five chemical markers namely three phenolic acids: caffeic acid (2), ferulic acid (5) and coumaric acid (4); one flavonol (6) one dihydrochalcone (8), one flavanone (7) and two flavano-3-ols (1/3) were selected for simultaneous quantitative determination. UV detection wavelengths were chosen based on UV spectrum of the markers. The phenolic acids had strongest UV absorption at 300, 309 and 322 nm, whereas flavanones at 284, 330 nm, flavonols had 254, 255 and 354 nm, dihydrocalcones 284 nm and finally flavan-3-ol, at 278 nm. Using the methods described, the phenolic compounds were detectable and quantifiable in the extracts of *T. portulacastrum* (Table 4) sampled with a high degree of sensitivity, as indicated by their limits of quantification and detection (Table 5). The limits of detection and quantification observed, along with the calculated recoveries, indicate this method's suitability for profiling phenolic compounds from the samples analyzed. The quantification of phenolic compounds using UHPLC-MS expressed as caffeic acid, ferulic acid, coumaric acid, rutin catechin, epicatechin, hesperidin equivalents, or other phenolic compounds has been reported in many papers.

Principal component analysis reveals associations in the quantity of metabolites in different cultivars forming the first association in shoot extracts (T01 and T02), followed by whole plant extracts (T04 and T03) and lastly the root association (T05 and T06). However, the white flower cultivar was found to have higher polyphenol content and thus higher antioxidant potential than the purple flower.

4. Discussion

Novel anticancer compounds such as bioactive O-Prenyl, acetylenic metabolites, coumarin derivatives and other marine-based anticancer drugs are produced by plants (Jimeno et al., 2004; Nigam et al., 2019). These metabolites which are majorly products of secondary metabolism offer extended pharmacological values, and could minimize carcinogenic effects by suppressing the proliferation and survival of cancer cells (Choudhari et al., 2020; Detsi et al., 2017). This study has revealed several natural compounds such as chlorogenic acid (among otherhydroxycinnamic acids), flava-3-ol such as epigallocatechin, byakangelicin, xanthotoxin, apaensin (coumarins), acetoxy-6-gingeroland so on from *T. portulacastrum* with potential antioxidant and inhibitory effects on cancer invasion and malignant growths which had not been previously identified from this plant although they could be sourced from elsewhere.

Hydroxycinnamic acids are an important source of antioxidants due to their ubiquitous occurrence in plants. As a result of antioxidant activity, they have been found to prevent various diseases associated with oxidative stress, such as cancer and cardiovascular diseases. There has been reported data that hydroxycinnamic acids have potential inhibitory effect on cancer invasion and metastasis (Weng and Yen, 2012). Hydroxycinnamic acids increase cytotoxicity and apostasis of DU145 of prostate cancer (Szliszka et al., 2011). p-Coumaric acid decreased numbers of viable MDA-MB 468 and HBL 100 breast cells, colon-derived SW480 cells and human colonic epithelial cells (Tehami et al., 2023). Kampa et al. (2004) studied the antiproliferative action of protocatechuic acid on T47D human breast cancer cells. The results showed a time and dose-dependent inhibitory effect on cell growth. The antioxidative activity of these phenolic acids in T47D cells does not coincide with their inhibitory effect on tumoral proliferation. Gallic acid suppresses cell viability, proliferation, invasion and angiogenesis in human glioma cells (Lu et al., 2010). Previous reports indicate that ADAM17 contributes to cancer cell invasiveness through activation of PI3K/Akt (Zheng et al., 2009). Ferulic acid increases free radical scavenging and cytotoxicity against SNU638 and AGS cell lines of gastric cancer (Lu et al., 2010; Kim et al., 2011).

Gallic acid is also cytotoxic against certain cancer cells, without harming normal cells (Lu et al., 2010). Gallic acid inhibited cancer invasion/metastasis in vitro and in vivo of Gastric adenocarcima, AGS inhibit the activity or expression of MMP-2/-9;F-actin, PI3K;p38; NF-kB through the modulation of the activities/ phosphorylation of Cdc42; Ras; Rac1; RhoA; RhoB. Epigallocatechin gallate has been previously used as a strong inhibition of the gelatinolytic activity of MMP-9 (Demeule et al., 2000; Gan et al., 2018) and was one of the compounds identified from *T. portulacastrum.* In vitro study of epicatechin demonstrated growth inhibition against human cancer cells in the colon (IC_{50} μM = 60); prostate (IC_{50} μM = 8.9); ovarian (IC_{50} μM = 7.9) (Park et al., 2004).

Additionally, in vitro cytotoxicity of (-)-epicatechin gallate (ECG) to cancer and normal cells from the human oral cavity: Breast (IC_{50} μM = 350.0); colon (IC_{50} μM = 1000); lung (IC_{50} μM = 78.0) led to induction of apoptosis of cancer cell lines (Babich et al., 2005). Epigallocatechin inhibited growth and induced apoptosis in human cancer cell lines according to the in vitro study for the following cancer cells: Breast (IC_{50} μM = 22.0); colon (IC_{50} μM = 75.0); lung (IC_{50} μM = 70.0) (Yang et al., 1998). Quercetin, by attenuating prostate cancer cell survival led to

Table 5
Content and antioxidant properties of the cultivars.

Sample	Polyphenols (mg GAE/L)	Flavonols (mg QE/L)	Flavanols (mg CE/L)	FRAP (umol AAE/L)	DPPH (umol TE/L)	TEAC (umol TE/L)	Alkaloids (mg/L)
#	*Av* ±SE	*Av* ±SE	*Av* ±SE	*Av* ±SE	*Av* ±SE	*Av* ±SE	*Av* ±SE
TO1	199.6 ± 5.7	121.9 ± 1.8	40.6 ± 0.0	1047.2 ± 39.7	1258.6 ± 114.0	3766.1 ± 180.7	N.D.
TO2	101.7 ± 4.4	65.9 ± 2.7	22.0 ± 0.0	431.9 ± 9.3	652.0 ± 21.8	1732.7 ± 65.3	N.D.
TO3	154.8 ± 1.9	76.6 ± 7.8	25.5 ± 0.0	517.3 ± 18.2	775.7 ± 51.2	2520.8 ± 32.9	N.D.
TO4	157.4 ± 5.0	93.9 ± 8.2	31.3 ± 0.0	614.2 ± 8.930701	704.1 ± 13.1	2270.4 ± 84.2	N.D.
TO5	43.4 ± 0.6	15.2 ± 0.7	5.1 ± 0.0	195.0966 ± 29.9	528.2 ± 15.4	1335.4 ± 30.4	N.D.
TO6	13.0 ± 1.6	6.7 ± 0.8	2.2 ± 0.0	58.9 ± 16.1	505.5 ± 50.8	468.0 ± 19.6	N.D.

GAE = Gallic acid equivalents, QE = Quercetin equivalents, CE = Catechin equivalents, AAE = Ascorbic acid equivalents, TE = Trolox equivalents, N.D. = none detected.

inhibition of antiapoptotic pathways in the human PCa cell lines, LNCaP, DU-145, and PC-3. Luteolin through attenuation of epithelial-mesenchymal transition induced by TGF-β1 in lung cancer cells in the human adenocarcinoma cell line A549 (Chen et al., 2013). Procyanidins consumption was implicated in improved antioxidant status and delayed tumor in animal test systems in vitro according to various studies by (Bomser et al., 1999; Packer et al., 1999; Rauf et al., 2019; Yang et al., 2021). Magnolol is a promising natural compound for the treatment of gastric cancer and may be a potential candidate for in vivo studies of monotherapies or combination antitumor therapies (Rasul et al., 2012). Coumarins and its derivatives with potent in vitro/in vivo biological activity were implicated as promising anticancer compounds (Detsi et al., 2017; Kontogiorgis et al., 2012).

Other anticancer compounds found in *T. portulacastrum* is chlorogenic acid. This compound has been found to inhibit matrix metalloproteinase (MMP-9) activity, which in turn would be a potential means of controlling the growth and invasiveness of tumors. Chlorogenic acid was confirmed to possess cross-inhibitory effect on MMP-9 by the artificial substrate and gelatin zymography (Weng and Yen, 2012). It was further observed that chlorogenic acid does not have cytotoxic effects on cellular proliferation, when Hep3B cells were treated with various concentrations of chlorogenic acid. Chlorogenic acid inhibits sphingosine-1- phosphate-induced ERK phosphorylation in U-87 glioma cells (Belkaid et al., 2006).

In this study, flavan-3-ols were the most abundant group of compounds especially in the *T. portulacastrum* root (purple flower) and *T. portulacastrum* root (white flower). Since many flava-3-ol were detected especially in the *T. portulacastrum* root (purple flower) and *T. portulacastrum* root (white flower) cultivars, the potential of these cultivars for anticancer activities is profound. Paradoxically, the total polyphenol content was low compared to that of *T. portulacastrum* shoot (white flower). The LC–MS metabolomics encounters some challenges during data analysis, metabolite annotation, and identifying biological molecules from mass spectral data Principal component analysis (PCA) is a powerful chemometric tool that pinpoint the effects of technical variance in metabolic profile analysis and evaluate the quality of the data (Miller and Miller, 2010). Following the pre-processing LC–MS data of the *portulacastrum* species PCA was applied to explore sample clustering for both positive and negative ion modes data, and to study the variation within the *T. portulacastrum* samples. Using PCA, the data's dimensionality is decreased while most data sets variation is preserved. This dimensionality reduction is achieved through finding the key directions-known as components, along which the data's maximum variance occurs. The remaining principal components, having minor effects on the model, were discarded. This analysis successfully differentiated T01 and T02 from T03 and T04, and both differentiated from T05 and T06, (Fig. 5) establishing three reliable clustered groups, based on nature and the levels of metabolites. That is metabolites could be identified along shoot, whole plant and root with disregard to the color. T01 and T02 shared most metabolites and so are the other groupings. However the white flower cultivar was found to have higher polyphenol content and thus higher antioxidant potential than the purple flower (Fig. 6).

Rapid decreases in cell index (CI) values observed at higher extract percentages determined by the xCELLigence real time cell analyzer are highly indicative of cell death as the rapid reduction in electrical impedance measurement is an indication of a decrease in direct contact of the cellular monolayer with the surface; increases in CI represents the inverse of this. This is a clear manifestation of the diversity, enormity and biological activity of anticancer metabolites in the tested extracts of *T. portulacastrum*. The calculated IC_{50} values determined for each extract with relative goodness of fit represented by the R^2 value suggest that all extracts showed high levels of cytotoxicity as determined by the xCELLigence apart from T05 and T06. Also, the responses observed 48 h post exposure and the relative IC_{50} values determined using the area under the curve analysis during this period using the concentration range of 0.16–2.5 % suggest that extracts of *T. portulacastrum* have inhibitory effects against cancer, and are rich in antioxidant compounds.

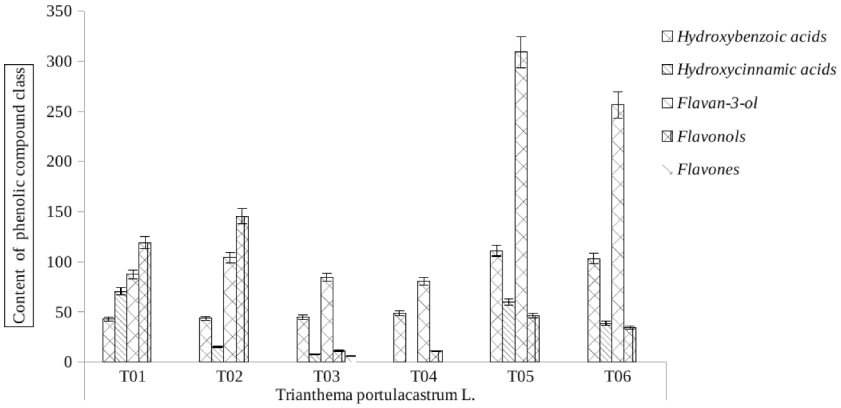

Fig. 5. Amount of phenolic compounds in T01 = *T. portulacastrum* shoot (white flower), T02 = *T portulacastrum* shoot (purple flower), T03 = *T portulacastrum* whole plant (white flower), T04 = *T portulacastrum* whole plant (purple flower), T05 = *T portulacastrum* root (white flowered), T06 = *T portulacastrum* root (purple flower).

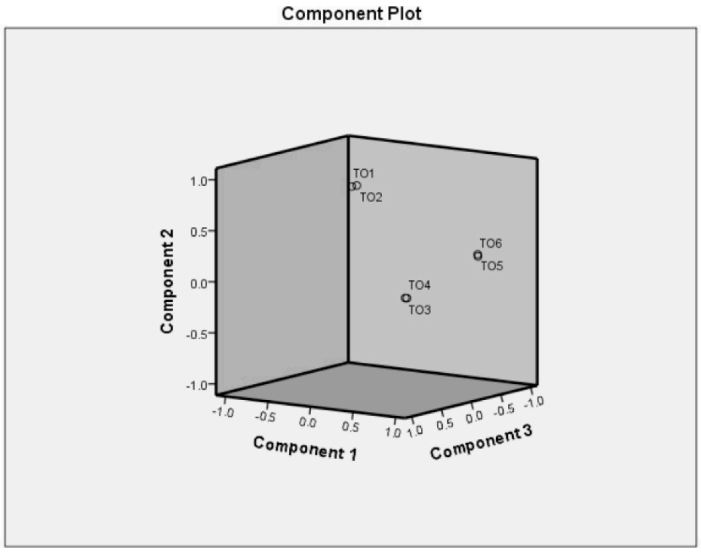

Fig. 6. Principal component analysis reveals associations in the amount of metabolites in different cultivars.

5. Conclusion

This study shows that *T. portulacastrum* is a promising vegetable due to its diverse anticancer compounds and other chemicals with extended therapeutic benefits which could be used to develop plant-based anti-cancer drugs. It further suggests that phytonutrients from the plant could be used to improve the biological values of food. High levels of cytotoxicity was exhibited by shoot and whole plant than root. The findings based on PCA shows that clusters or associations of metabolites could be identified along shoot, whole plant and root with disregard to the color in the cultivars. The LCMS has revealed so many metabolites which had not been previously identified from *T. portulacastrum* of which a few of them have previously demonstrated anticancer and antioxidant properties. The LC–MS has also tried to distinguish between cultivars based on plant parts since metabolites could be identified along shoot, whole plant and root. Other analytical techniques should be explored to isolate pure compounds from the plant to foster repeatability and ensure therapeutic integrity of the characterized metabolites.

CRediT authorship contribution statement

Muhali Olaide Jimoh: Conceptualization, Data curation, Formal analysis, Investigation, Validation, Writing – original draft, Writing – review & editing. **Mahboob Adekilekun Jimoh:** Conceptualization, Supervision, Writing – review & editing. **Nasifu Kerebba:** Data curation, Formal analysis, Writing – original draft, Writing – review & editing, Methodology, Software. **Olalekan Olanrewaju Bakare:** Methodology, Writing – review & editing. **Comfort Titilayomi Senjobi:** Writing – review & editing. **Sefiu Adekilekun Saheed:** Writing – review & editing. **Rose Kadye:** Investigation, Writing – review & editing. **Earl Prinsloo:** Data curation, Investigation, Methodology, Writing – review & editing. **Charles Petrus Laubscher:** Conceptualization, Funding acquisition, Supervision, Writing – review & editing.

Declaration of competing interest

All authors wish to state that there is no interest to declare.

Acknowledgments

Authors wish to thank the Cape Peninsula University of Technology for supporting this study.

References

Abuzaid, H., Amin, E., Moawad, A., Ramadan Abdelmohsen, U., Hetta, M., Mohammed, R., 2020. Liquid chromatography high-resolution mass spectrometry analysis, phytochemical and biological study of two aizoaceae plants: a new kaempferol derivative from Trianthema portulacastrum L. 10.4103/pr.pr_119_19.

Algharib, M., 2010. ChemInform abstract: reaction of acylcarbonitrile oxides with 3,4-dihydro-6,7- dimethoxyisoquinoline derivatives. ChemInform 27. https://doi.org/10.1002/CHIN.199632054 no-no.

Altmann, D.M., 2018. A Nobel prize-worthy pursuit: cancer immunology and harnessing immunity to tumour neoantigens. Immunology 155, 283–284. https://doi.org/10.1111/imm.13008.

Arnedos, M., Soria, J.C., Andre, F., Tursz, T., 2014. Personalized treatments of cancer patients: a reality in daily practice, a costly dream or a shared vision of the future from the oncology community? Cancer Treat. Rev. 40, 1192–1198. https://doi.org/10.1016/J.CTRV.2014.07.002.

Atale, N., Gupta, S., Yadav, U.C.S., Rani, V., 2014. Cell-death assessment by fluorescent and nonfluorescent cytosolic and nuclear staining techniques. J. Microsc. 255, 7–19. https://doi.org/10.1111/JMI.12133.

Babich, H., Krupka, M.E., Nissim, H.A., Zuckerbraun, H.L., 2005. Differential in vitro cytotoxicity of (-)-epicatechin gallate (ECG) to cancer and normal cells from the human oral cavity. Toxicol. Vitro 19, 231–242. https://doi.org/10.1016/j.tiv.2004.09.001.

Belkaid, A., Currie, J.C., Desgagnés, J., Annabi, B., 2006. The chemopreventive properties of chlorogenic acid reveal a potential new role for the microsomal glucose-6-phosphate translocase in brain tumor progression. Cancer Cell Int. 6, 1–12. https://doi.org/10.1186/1475-2867-6-7.

Bomser, J.A., Singletary, K.W., Wallig, M.A., Smith, M.A.L., 1999. Inhibition of TPA-induced tumor promotion in CD-1 mouse epidermis by a polyphenolic fraction from grape seeds. Cancer Lett. 135, 151–157.

Branch, S.K., 2005. Guidelines from the International Conference on Harmonisation (ICH). J. Pharm. Biomed. Anal. 38, 798–805. https://doi.org/10.1016/J.JPBA.2005.02.037.

Bray, F., Laversanne, M., Weiderpass, E., Soerjomataram, I., 2021. The ever-increasing importance of cancer as a leading cause of premature death worldwide. Cancer 127, 3029–3030. https://doi.org/10.1002/CNCR.33587.

Chen, K.C., Chen, C.Y., Lin, C.J., Yang, T.Y., Chen, T.H., Wu, L.C., Wu, C.C., 2013. Luteolin attenuates TGF-β1-induced epithelial-mesenchymal transition of lung cancer cells by interfering in the PI3K/Akt-NF-κB-Snail pathway. Life Sci. 93, 924–933. https://doi.org/10.1016/j.lfs.2013.10.004.

Choudhari, A.S., Mandave, P.C., Deshpande, M., Ranjekar, P., Prakash, O., 2020. Phytochemicals in cancer treatment: from preclinical studies to clinical practice. Front. Pharmacol. 10 https://doi.org/10.3389/FPHAR.2019.01614/FULL.

Chrzanowska, M., Grajewska, A., Rozwadowska, M.D., 2016. Asymmetric synthesis of isoquinoline alkaloids: 2004-2015. Chem. Rev. 116, 12369–12465. https://doi.org/10.1021/ACS.CHEMREV.6B00315/ASSET/IMAGES/LARGE/CR-2016-00315H_0090.JPEG.

Cox, T.R., 2021. The matrix in cancer. Nat. Rev. Cancer 21 (4), 217–238. https://doi.org/10.1038/s41568-020-00329-7, 202121.

Davis, L.E., Shalin, S.C., Tackett, A.J., 2019. Current state of melanoma diagnosis and treatment. Cancer Biol. Ther. 20, 1366–1379. https://doi.org/10.1080/15384047.2019.1640032.

Deevanhxay, P., Suzuki, M., Maeshibu, N., Li, H., Tanaka, K., Hirose, S., 2009. Simultaneous characterization of quaternary alkaloids, 8-oxoprotoberberine alkaloids, and a steroid compound in Coscinium fenestratum by liquid

chromatography hybrid ion trap time-of-flight mass spectrometry. J. Pharm. Biomed. Anal. 50, 413–425. https://doi.org/10.1016/j.jpba.2009.05.023.
Demeule, M., Brossard, M., Pagë, M., Gingras, D., Bëliveau, R., 2000. Matrix metalloproteinase inhibition by green tea catechins. Biochim. Biophys. Acta 1478, 51–60.
Detsi, A., Kontogiorgis, C., Hadjipavlou-Litina, D., 2017. Coumarin derivatives: an updated patent review (2015-2016). Expert. Opin. Ther. Pat. 27, 1201–1226. https://doi.org/10.1080/13543776.2017.1360284.
Dogara, A.M., Labaran, I., Yunusa, A., 2020. Ethnobotany of medicinal plants with antimalarial potential in Northern Nigeria. Ethnobot. Res. Appl. 19, 1–8.
Escobar-Avello, D., Lozano-Castellón, J., Mardones, C., Pérez, A.J., Saéz, V., Riquelme, S., Von Baer, D., Vallverdú-Queralt, A., 2019. Phenolic profile of grape canes: novel compounds identified by LC-ESI-LTQ-orbitrap-MS. Molecules 24. https://doi.org/10.3390/molecules24203763.
Fadelu, T., Rebbeck, T.R., 2021. The rising burden of cancer in low– and middle–Human Development Index countries. Cancer 127, 2864–2866. https://doi.org/10.1002/CNCR.33586.
Falade, T., Ishola, I.O., Akinleye, M.O., Oladimeji-Salami, J.A., Adeyemi, O.O., 2019. Antinociceptive and anti-arthritic effects of aqueous whole plant extract of Trianthema portulacastrum in rodents: possible mechanisms of action. J. Ethnopharmacol. 238 https://doi.org/10.1016/j.jep.2019.111831.
Filetti, V., Falzone, L., Rapisarda, V., Caltabiano, R., Eleonora Graziano, A.C., Ledda, C., Loreto, C., 2020. Modulation of microRNA expression levels after naturally occurring asbestiform fibers exposure as a diagnostic biomarker of mesothelial neoplastic transformation. Ecotoxicol. Environ. Saf. 198, 110640 https://doi.org/10.1016/J.ECOENV.2020.110640.
Gaddeyya, G., Kumar, R.P.K., 2015. Botanical description, eco-physiology and control of Trianthema portulacastrum Linn. J. Crop Weed 11, 47–54.
Gan, R.Y., Li, H.Bin, Sui, Z.Q., Corke, H., 2018. Absorption, metabolism, anti-cancer effect and molecular targets of epigallocatechin gallate (EGCG): an updated review. Crit. Rev. Food Sci. Nutr. 58, 924–941. https://doi.org/10.1080/10408398.2016.1231168.
Gao, H., Li, Q., 2023. Study on the spatial distribution of coumarins in Angelica dahurica root by MALDI-TOF-MSI. Phytochem. Anal. 34, 139–148. https://doi.org/10.1002/PCA.3186.
Genovese, S., Fiorito, S., Epifano, F., Alessandro Taddeo, V., 2015. A novel class of emerging anticancer compounds: oxyprenylated secondary metabolites from plants and fungi. Curr. Med. Chem. 22, 3426–3433.
Goger, F., Kose, Y.B., Goger, G, Demirci, F., 2015. Phytochemical characterization of phenolics by LC-MS and biological evaluation of Ajuga orientalis from Turkey. Bangladesh J. Pharmacol. 10, 639–644.
Hamidi, H., Lilja, J., Ivaska, J., 2017. Using xCELLigence RTCA instrument to measure cell adhesion. Bio Protoc. 7 https://doi.org/10.21769/bioprotoc.2646.
Harnly, J.M., Bhagwat, S., Lin, L.Z., 2007. Profiling methods for the determination of phenolic compounds in foods and dietary supplements. Anal. Bioanal. Chem. 389, 47–61.
Horai, H., Arita, M., Kanaya, S., Nihei, Y., Ikeda, T., Suwa, K., Ojima, Y., Tanaka, Kenichi, Tanaka, S., Aoshima, K., Oda, Y., Kakazu, Y., Kusano, M., Tohge, T., Matsuda, F., Sawada, Y., Hirai, M.Y., Nakanishi, H., Ikeda, K., Akimoto, N., Maoka, T., Takahashi, H., Ara, T., Sakurai, N., Suzuki, H., Shibata, D., Neumann, S., Iida, T., Tanaka, Ken, Funatsu, K., Matsuura, F., Soga, T., Taguchi, R., Saito, K., Nishioka, T., 2010. MassBank: a public repository for sharing mass spectral data for life sciences. J. Mass Spectrom. 45, 703–714. https://doi.org/10.1002/JMS.1777.
Howell, S., Shalet, S., 1998. Gonadal damage from chemotherapy and radiotherapy. Endocrinol. Metab. Clin. North Am. 27, 927–943. https://doi.org/10.1016/S0889-8529(05)70048-7.
Hussain, A., Khan, M.N., Iqbal, Z., Sajid, M.S., 2011. Anthelmintic activity of Trianthema portulacastrum L . and Musa paradisiaca L . against gastrointestinal nematodes of sheep. Vet. Parasitol. 179, 92–99. https://doi.org/10.1016/j.vetpar.2011.02.022.
Idris, O.A., Kerebba, N., Horn, S., Maboeta, M.S., Pieters, R., 2023. Phytochemical-based evidence of the health benefits of Bidens pilosa extracts and cytotoxicity. Chem. Africa. https://doi.org/10.1007/s42250-023-00626-2.
Igoli, J.O., Ogaji, O.G., Tor-Anyiin, T.A., Igoli, N.P., 2005. Traditional medicine practice amongst the Igede people of Nigeria. Part II. Afr. J. Tradit., Complement. Altern. Med. 2, 134–152.
Jimeno, J., Faircloth, G., Sousa-Faro, J.M.F., Scheuer, P., Rinehart, K., 2004. New marine derived anticancer therapeutics - a journey from the sea to clinical trials. Mar. Drugs 2, 14–29. https://doi.org/10.3390/md201014.
Jimoh, M.A., Jimoh, M.O., Bello, M., Raimi, I.O., Okunlola, G.O., Mkhwanazi, N., Laubscher, C.P., 2024. In vitro anti-HIV, cytotoxicity and nutritional analysis of Trianthema portulacastrum L. (Aizoaceae). BMC Complement. Med. Ther. 24, 1–11. https://doi.org/10.1186/s12906-023-04300-5.
Jimoh, M.O., Afolayan, A.J., Lewu, F.B., 2019. Antioxidant and phytochemical activities of Amaranthus caudatus L . harvested from different soils at various growth stages. Sci. Rep. 9, 12965. https://doi.org/10.1038/s41598-019-49276-w.
Kampa, M., Alexaki, V.-I., Notas, G., Nifli, A.-P., Nistikaki, A., Hatzoglou, A., Bakogeorgou, E., Kouimtzoglou, E., Blekas, G., Boskou, D., Gravanis, A., Castanas, E., 2004. Antiproliferative and apoptotic effects of selective phenolic acids on T47D human breast cancer cells: potential mechanisms of action. Breast Cancer Res. 6, R63–R74. https://doi.org/10.1186/BCR752.
Kappelmann, J., Klein, B., Geilenkirchen, P., Noack, S., 2017. Comprehensive and accurate tracking of carbon origin of LC-tandem mass spectrometry collisional fragments for 13C-MFA. Anal. Bioanal. Chem. 409, 2309–2326. https://doi.org/10.1007/S00216-016-0174-9.
Kim, S.J., Shin, J.Y., Cheong, T.C., Choi, I.J., Lee, Y.S., Park, S.H., Chun, K.H., 2011. Galectin-3 germline variant at position 191 enhances nuclear accumulation and activation of β-catenin in gastric cancer. Clin. Exp. Metastasis 28, 743–750. https://doi.org/10.1007/S10585-011-9406-8/FIGURES/4.
Kontogiorgis, C., Detsi, A., Hadjipavlou-Litina, D., 2012. Coumarin-based drugs: a patent review (2008 - present). Expert Opin. Ther. Pat. 22, 437–454. https://doi.org/10.1517/13543776.2012.678835.
Kruger, S., Ilmer, M., Kobold, S., Cadilha, B.L., Endres, S., Ormanns, S., Schuebbe, G., Renz, B.W., D'Haese, J.G., Schloesser, H., Heinemann, V., Subklewe, M., Boeck, S., Werner, J., Von Bergwelt-Baildon, M., 2019. Advances in cancer immunotherapy 2019 - latest trends. J. Exp. Clin. Cancer Res. 38, 1–11. https://doi.org/10.1186/S13046-019-1266-0/FIGURES/2.
Li, B., Zhang, X., Wang, J., Zhang, L., Gao, B., Shi, S., Wang, X., Li, J., Tu, P., 2014. Simultaneous characterisation of fifty coumarins from the roots of angelica dahurica by off-line two-dimensional high-performance liquid chromatography coupled with electrospray ionisation tandem mass spectrometry. Phytochem. Anal. 25, 229–240. https://doi.org/10.1002/PCA.2496.
Li, H.J., Deinzer, M.L., 2009. Proanthocyanidins in hops. Beer in Health and Disease Prevention, pp. 333–348. https://doi.org/10.1016/B978-0-12-373891-2.00032-8.
Lu, Y., Jiang, F., Jiang, H., Wu, K., Zheng, X., Cai, Y., Katakowski, M., Chopp, M., To, S.S. T., 2010. Gallic acid suppresses cell viability, proliferation, invasion and angiogenesis in human glioma cells. Eur. J. Pharmacol. 641, 102–107. https://doi.org/10.1016/J.EJPHAR.2010.05.043.
Ma, C., Xiao, S.yuan, Li, Z.guo, Wang, W., Du, L.jun, 2007. Characterization of active phenolic components in the ethanolic extract of Ananas comosus L. leaves using high-performance liquid chromatography with diode array detection and tandem mass spectrometry. J. Chromatogr. A 1165, 39–44. https://doi.org/10.1016/J.CHROMA.2007.07.060.
Mandal, A., Bishayee, A., 2015. Trianthema portulacastrum L. displays anti-inflammatory responses during chemically induced rat mammary tumorigenesis through simultaneous and differential regulation of NF-κB and Nrf2 signaling pathways. Int. J. Mol. Sci. 16, 2426–2445. https://doi.org/10.3390/ijms16022426.
Martin-Arjol, I., Bassas-Galia, M., Bermudo, E., Garcia, F., Manresa, A., 2010. Identification of oxylipins with antifungal activity by LC–MS/MS from the supernatant of pseudomonas 42A2. Chem. Phys. Lipids 163, 341–346. https://doi.org/10.1016/J.CHEMPHYSLIP.2010.02.003.
Miller, J.N., Miller, J.C., 2010. Statistics and Chemometrics for Analytical Chemistry, 6th edition. ed. Pearson Education Limited, Edinburgh Gate Harlow Essex CM20 2JE England.
Molnár, M., Treuerne Balázs, K.E., Madarász, Z., Nyerges, M., 2022. New reactions of 3,4-dihydro-6,7-dimethoxyisoquinoline ylide with nitrile derivatives. J. Heterocycl. Chem. 59, 1635–1650. https://doi.org/10.1002/JHET.4496.
Nigam, M., Suleria, H.A.R., Farzaei, M.H., Mishra, A.P., 2019. Marine anticancer drugs and their relevant targets: a treasure from the ocean. DARU J. Pharm. Sci. 27 (1 27), 491–515. https://doi.org/10.1007/S40199-019-00273-4, 2019.
NIST, 2021. Mass Spectrometry Data Center, National Institute of Standards and Technology (NIST) [WWW Document]. http://chemdata.nist.gov/. (accessed 6.25.23).
Packer, L., Rimbach, G., Virgili, F., 1999. Antioxidant activity and biologic properties of a procyanidin-rich extract from pine (Pinus maritima) bark, pycnogenol.
Pardoll, D.M., 2012. The blockade of immune checkpoints in cancer immunotherapy. Nat. Rev. Cancer 12, 252–264. https://doi.org/10.1038/NRC3239.
Park, K.D., Lee, S.G., Kim, S.U., Kim, S.H., Sun, W.S., Cho, S.J., Jeong, D.H., 2004. Anticancer activity of 3-O-acyl and alkyl-(-)-epicatechin derivatives. Bioorg. Med. Chem. Lett. 14, 5189–5192. https://doi.org/10.1016/j.bmcl.2004.07.063.
Park, S.Y., Jung, M.Y., 2016. UHPLC-ESI-MS/MS for the quantification of eight major gingerols and shogaols in ginger products: effects of ionization polarity and mobile phase modifier on the sensitivity. J. Food Sci. 81, C2457–C2465. https://doi.org/10.1111/1750-3841.13429.
Pretsch, E., Bühlmann, P., Badertscher, M., 2009. Structure determination of organic compounds: tables of spectral data. Structure Determination of Organic Compounds: Tables of Spectral Data, pp. 1–433. https://doi.org/10.1007/978-3-540-93810-1/COVER.
Qing, Z.X., Cheng, P., Liu, X.Bin, Liu, Y.S., Zeng, J.G., 2015. Systematic identification of alkaloids in Macleaya microcarpa fruits by liquid chromatography tandem mass spectrometry combined with the isoquinoline alkaloids biosynthetic pathway. J. Pharm. Biomed. Anal. 103, 26–34. https://doi.org/10.1016/J.JPBA.2014.11.002.
Rasul, A., Yu, B., Khan, M., Zhang, K., Iqbal, F., Ma, T., Yang, H., 2012. Magnolol, a natural compound, induces apoptosis of SGC-7901 human gastric adenocarcinoma cells via the mitochondrial and PI3K/Akt signaling pathways. Int. J. Oncol. 40, 1153–1161. https://doi.org/10.3892/ijo.2011.1277.
Rauf, A., Imran, M., Abu-Izneid, T., Iahtisham-Ul-Haq Patel, S., Pan, X., Naz, S., Sanches Silva, A., Saeed, F., Rasul Suleria, H.A., 2019. Proanthocyanidins: a comprehensive review. Biomed. Pharmacother. 116, 108999 https://doi.org/10.1016/J.BIOPHA.2019.108999.
Reiser, K.M., 2007. Extracellular matrix. Encyclopedia of Gerontology, pp. 555–564. https://doi.org/10.1016/B0-12-370870-2/00070-6.
Royal Botanic Gardens, K. (K), 2023. Trianthema portulacastrum Linn. (family Aizoaceae) [WWW Document], 1985. In: Burkill, H.M. (Ed.), The Useful Plants of West Tropical Africa. Vol 1URL. https://plants.jstor.org/stable/10.5555/al.ap.upwta.1_119. accessed 3.8.23.
Sawada, Y., Nakabayashi, R., Yamada, Y., Suzuki, M., Sato, M., Sakata, A., Akiyama, K., Sakurai, T., Matsuda, F., Aoki, T., Hirai, M.Y., Saito, K., 2012. RIKEN tandem mass spectral database (ReSpect) for phytochemicals: a plant-specific MS/MS-based data resource and database. Phytochemistry 82, 38–45. https://doi.org/10.1016/j.phytochem.2012.07.007.
Serag, A., Baky, M.H., Döll, S., Farag, M.A., 2020. UHPLC-MS metabolome based classification of umbelliferous fruit taxa: a prospect for phyto-equivalency of its

different accessions and in response to roasting. RSC Adv. 10, 76–85. https://doi.org/10.1039/C9RA07841J.
Seraphin, T.P., Joko-Fru, W.Y., Kamaté, B., Chokunonga, E., Wabinga, H., Somdyala, N.I. M., Manraj, S.S., Ogunbiyi, O.J., Dzamalala, C.P., Finesse, A., Korir, A., N'Da, G., Lorenzoni, C., Liu, B., Kantelhardt, E.J., Parkin, D.M., 2021. Rising prostate cancer incidence in Sub-Saharan Africa: a trend analysis of data from the African cancer registry network. Cancer Epidemiol. Biomarkers Prev. 30, 158–165. https://doi.org/10.1158/1055-9965.EPI-20-1005.
Shaltout, K., Ahmed, D.A., Baraka, D.M., Shehata, M.N., Ahmed, D., Arief, O.M., 2013. Distributional behavior and growth performance of Trianthema portulacastrum L. (Aizoaceae) in Nile Delta. Egypt. J. Bot. 183–199, 3rd International Conference.
Shivhare, M.K., Singour, P.K., Chaurasiya, P.K., Pawar, R.S., 2012. Trianthema portulacastrum Linn. (Bishkhapra). Pharmacogn. Rev. 6 (132) https://doi.org/10.4103/0973-7847.99947.
Siddiq, A., Dembitsky, V., 2008. Acetylenic anticancer agents. AntiCancer Agents Med. Chem. 8, 132–170. https://doi.org/10.2174/187152008783497073.
Spínola, V., Llorent-Martínez, E.J., Gouveia, S., Castilho, P.C., 2014. Myrica faya: a new source of antioxidant phytochemicals. J. Agric. Food Chem. 62, 9722–9735. https://doi.org/10.1021/jf503540s.
Stefanowicz-Hajduk, J., Ochocka, J.R., 2020. Real-time cell analysis system in cytotoxicity applications: usefulness and comparison with tetrazolium salt assays. Toxicol. Rep. 7, 335–344. https://doi.org/10.1016/J.TOXREP.2020.02.002.
Sukalingam, K., Ganesan, K., Xu, B., 2017. Trianthema portulacastrum L. (giant pigweed): phytochemistry and pharmacological properties. Phytochem. Rev. 16, 461–478. https://doi.org/10.1007/s11101-017-9493-5.
Sunder, A.S., Reddy, A.R.N., Kiran, G., Thirumurugu, S., 2010. Anti-hyperlipidemic and antioxidant activity of methanolic extract of Trianthema portulacastrum in rats fed a high-fat diet. J. Herbs. Spices Med. Plants 16, 1–10.
Sung, H., Ferlay, J., Siegel, R.L., Laversanne, M., Soerjomataram, I., Jemal, A., Bray, F., 2021. Global Cancer Statistics 2020: GLOBOCAN estimates of incidence and mortality worldwide for 36 cancers in 185 countries. CA Cancer J. Clin. 71, 209–249. https://doi.org/10.3322/CAAC.21660.
Szliszka, E., Czuba, Z.P., Bronikowska, J., Mertas, A., Paradysz, A., Krol, W., 2011. Ethanolic extract of propolis augments TRAIL-induced apoptotic death in prostate cancer cells. Evid.-based Complement. Altern. Med. https://doi.org/10.1093/ecam/nep180, 2011.
Tehami, W., Nani, A., Khan, N.A., Hichami, A., 2023. New insights into the anticancer effects of p-coumaric acid: focus on colorectal cancer. Dose-Response 21. https://doi.org/10.1177/15593258221150704/ASSET/IMAGES/LARGE/10.1177_15593258221150704-FIG3.JPEG.
Tsimogiannis, D., Oreopoulou, V., 2007. Defining the role of flavonoid structure on cottonseed oil stabilization: study of A- and C-ring substitution. JAOCS, J. Am. Oil Chem. Soc. 84, 129–136. https://doi.org/10.1007/S11746-006-1016-2/FIGURES/4.
Wei, C., Crowne, E., 2019. The impact of childhood cancer and its treatment on puberty and subsequent hypothalamic pituitary and gonadal function, in both boys and girls. Best Pract. Res. Clin. Endocrinol. Metab. 33, 101291 https://doi.org/10.1016/J.BEEM.2019.101291.
Weng, C.J., Yen, G.C., 2012. Chemopreventive effects of dietary phytochemicals against cancer invasion and metastasis: phenolic acids, monophenol, polyphenol, and their derivatives. Cancer Treat. Rev. https://doi.org/10.1016/j.ctrv.2011.03.001.
Wu, H., Guo, J., Chen, S., Liu, X., Zhou, Y., Zhang, X., Xu, X., 2013. Recent developments in qualitative and quantitative analysis of phytochemical constituents and their metabolites using liquid chromatography–mass spectrometry. J. Pharm. Biomed. Anal. 72, 267–291. https://doi.org/10.1016/J.JPBA.2012.09.004.
Yang, G., Liao, J., Kim, K., Yurkow, E., Carcinogenesis, C.Y.-., 1998, undefined, 1998. Inhibition of growth and induction of apoptosis in human cancer cell lines by tea polyphenols. academic.oup.com 19, 611–616.
Yang, H., Li, Q., 2022. Simultaneous determination of the content of isoimperatorin, imperatorin, oxypeucedanin, xanthotoxol and byakangelicin in Angelica dahurica by HPTLC scanning. J. Chromatogr. Sci. https://doi.org/10.1093/CHROMSCI/BMAC087.
Yang, H., Tuo, X., Wang, L., Tundis, R., Portillo, M.P., Simal-Gandara, J., Yu, Y., Zou, L., Xiao, J., Deng, J., 2021. Bioactive procyanidins from dietary sources: the relationship between bioactivity and polymerization degree. Trends Food Sci. Technol. 111, 114–127. https://doi.org/10.1016/J.TIFS.2021.02.063.
Zavattaro, M., Lanfranco, F., Salvagno, F., Motta, G., Sestero, M., Marinelli, L., Canosa, S., Revelli, A., 2021. Gonadal failure and infertility in cancer survivors: clinical management and strategies for prevention. Front. Horm. Res. 54, 58–68. https://doi.org/10.1159/000515460.
Zeb, A., 2015. A reversed phase HPLC-DAD method for the determination of phenolic compounds in plant leaves. Anal. Methods 7, 7753–7757. https://doi.org/10.1039/C5AY01402F.
Zhang, Q.Y., Wang, F.X., Jia, K.K., Kong, L.D., 2018. Natural product interventions for chemotherapy and radiotherapy-induced side effects. Front. Pharmacol. 9, 1253. https://doi.org/10.3389/FPHAR.2018.01253/BIBTEX.
Zheng, X., Jiang, F., Katakowski, M., Zheng, G.Z., Lu, Q.E., Chopp, M., 2009. ADAM17 promotes breast cancer cell malignant phenotype through EGFR-PI3K-AKT activation. Cancer Biol. Ther. 8, 1045–1054. https://doi.org/10.4161/cbt.8.11.8539.
Zubarev, R.A., Makarov, A., 2013. Orbitrap Mass Spectrometry. Anal. Chem. 85, 5288–5296. https://doi.org/10.1021/AC4001223.